Adaptive Instantiation of the Protocol Interference Model in Wireless Networked Sensing and Control

Hongwei Zhang, Xin Che, Xiaohui Liu, Xi Ju, Wayne State University

Interference model is the basis of MAC protocol design in wireless networked sensing and control, and it directly affects the efficiency and predictability of wireless messaging. To exploit the strengths of both the physical and the protocol interference models, we analyze how network traffic, link length, and wireless signal attenuation affect the optimal instantiation of the protocol model. We also identify the inherent tradeoff between reliability and throughput in the model instantiation. Our analysis sheds light on the open problem of efficiently optimizing the protocol model instantiation. Based on the analytical results, we propose the physical-ratio-K (PRK) interference model as a reliability-oriented instantiation of the protocol model. Via analysis, simulation, and testbed-based measurement, we show that PRK-based scheduling achieves a network throughput very close to (e.g., 95%) what is enabled by physical-model-based scheduling while ensuring the required packet delivery reliability. The PRK model inherits both the high fidelity of the physical model and the locality of the protocol model, thus it is expected to be suitable for distributed protocol design. These findings shed new light on wireless interference models; they also suggest new approaches to MAC protocol design in the presence of uncertainties in network and environmental conditions as well as application QoS requirements.

Categories and Subject Descriptors: C.2.0 [**Computer-Communication Networks**]: General

General Terms: Design, Performance, Experimentation, Measurement, Algorithms

Additional Key Words and Phrases: Wireless interference model, protocol model, physical model, throughput, reliability, local adaptation, analysis, measurement, simulation, control theory

1. INTRODUCTION

With the development of networked embedded sensing and control, wireless networks are increasingly applied to mission-critical applications such as industrial monitoring and control [Chintalapudi and Venkatraman 2008]. This is evidenced by the recent industry standards such as WirelessHART [Chen et al. 2010] and ISA SP100.11a [ISA SP100.11a] which target wireless networked sensing and instrumentation. In supporting real-time, mission-critical tasks, these wireless networks are required to ensure real-time, reliable data delivery. Nonetheless, wireless communication is subject to various dynamics and uncertainties. Due to the broadcast nature of wireless communication, in particular, concurrent transmissions may interfere with one another and introduce co-channel interference. Co-channel interference not only reduces the reliability and throughput of wireless networks, it also increases the variability and uncertainty in data communication [Tobagi and Kleinrock 1975; Zhou et al. 2005; Zhang et al. 2009]. Therefore, effectively scheduling concurrent transmissions to control co-channel interference has become critical for enabling reliable, predictable wireless communication.

A basis of interference control is the interference model which *predicts* whether a set of concurrent transmissions may interfere with one another. Two commonly used models are the physical interference model and the protocol interference model [Gupta and Kumar 2000]. In the physical model, a set of concurrent transmissions $(S_i, R_i), i = 1 \dots N$, are regarded as not interfering with one another if the following conditions hold:

$$\frac{P(S_i, R_i)}{N_i + \sum_{j=1 \dots N, j \neq i} P(S_j, R_i)} \geq \gamma_0, \;\; i = 1 \dots N,$$

This work is supported in part by NSF awards CNS-1136007, CNS-1054634, GENI-1890, and GENI-1633, as well as grants from Ford Research and GM Research. An extended abstract containing some preliminary results of this paper appeared in IEEE SECON 2010.

Hongwei Zhang, Xin Che, Xiaohui Liu, and Xi Ju are with the Department of Computer Science, Wayne State University, U.S.A. E-mail: {hongwei,chexin,xiaohui,xiju}@wayne.edu.

where $P(S_i, R_i)$ and $P(S_j, R_i)$ is the strength of signals reaching the receiver R_i from the transmitter S_i and S_j respectively, N_i is the background noise power at receiver R_i, and γ_0 is the signal-to-interference-plus-noise-ratio (SINR) threshold required to ensure a certain link reliability[1]. In the protocol model, a transmission from a node S to its receiver R is regarded as not being interfered by a concurrent transmitter C if

$$D(C, R) \geq K \times D(S, R),$$

where $D(C, R)$ and $D(S, R)$ is the geographic distance from C and S to R respectively, and K is a constant number.[2]. For simplicity, we also call the physical model the *SINR model* and the protocol model the *ratio-K model* in this paper, and we regard scheduling based on the SINR model and the ratio-K model SINR-based scheduling and ratio-K-based scheduling respectively.

The SINR model is based on communication theory, and it can be regarded as an instantiation of the graded-SINR model [Maheshwari et al. 2008] for satisfying certain minimum link reliability. The SINR model is a high fidelity model in general, but the interference relations defined by it are non-local and combinatorial. This is because whether one transmission interferes with another is modeled as *explicitly* depending on all the other transmissions in the network. Accordingly, SINR-based scheduling usually requires network-wide coordination. Since the coordination delay slows down protocol convergence [Brar et al. 2008; Yi et al. 2007] and increases uncertainty [Ying and Shakkottai 2009], it is difficult to use the SINR model in *distributed* protocol design. This is especially the case when network traffic pattern and environmental conditions are dynamic and potentially unpredictable.

Unlike the SINR model, the ratio-K model defines local, pair-wise/non-combinatorial interference relations where interference is regarded as existent only between nodes in a local neighborhood. Accordingly, the ratio-K model is suitable for distributed protocol design since ratio-K-based scheduling only requires coordination among nodes in their local neighborhood. The locality of ratio-K-based scheduling can also enable agile protocol adaptation for addressing the challenges of unpredictable traffic pattern and environmental dynamics. Nonetheless, the ratio-K model is an approximate model in nature, and it does not ensure reliable data delivery in general. For instance, the RTS-CTS-based channel access control can only enable a data delivery ratio of $\sim$50% in our field wireless sensor networks [Arora et al. 2005; Zhang et al. 2007]; via testbed-based measurement study of event-detection sensor networks, Choi et al. have also shown that CSMA- and RTS-CTS-based channel access control mechanisms may only enable a data delivery ratio of 16.9% and 36.8% respectively [Choi et al. 2010].

To enable the design of distributed MAC protocols for agile, predictable interference control, an *open question* is whether it is possible to develop an interference model that has both the locality of the ratio-K model and the high fidelity of the SINR model. Given that the ratio-K model is local and can enable agile, distributed protocols, we explore the possibility of extending the ratio-K model to preserve its locality while addressing the low performance issue of ratio-K-based scheduling. To this end, we first study the behavior of ratio-K-based scheduling, and a summary of our findings are as follows:

— We analyze how network traffic load, link length, and wireless signal attenuation affect the effective instantiation of the ratio-K model. We find that fixing K to a constant number, as in most existing studies [Chafekar et al. 2008; Maheshwari et al. 2008; Moscibroda et al. 2006], can lead to significant performance loss when network and environmental settings change. For instance, deviation from the optimal K by up to 1 can cause up to 68% throughput loss, and fixing K to 2 may lead to a link reliability less than 80%. These findings suggest that, when designing and

[1]By "link reliability", we mean the probability for a packet to be correctly received by its receiver(s) without errors; in this paper, we only consider packet transmission errors due to perturbations to data packet signals that are caused by background noise and/or interference signals.

[2]We replace the original notation of $(1 + \Delta)$ [Gupta and Kumar 2000] with K for simplicity. Also note that the commonly used K-hop model [Sharma et al. 2006] is a special case of the protocol model in geometric graphs.

evaluating ratio-K-based scheduling algorithms, it is important to choose the right parameter K according to network and environmental conditions.

— We also find that there is inherent tradeoff between reliability and throughput when instantiating the ratio-K model. Maximum network throughput is usually achieved not at the minimum K for ensuring certain link reliability, but at a smaller K. For instance, $\sqrt{2}$ is the optimal K for maximizing throughput in many scenarios, but, with non-negligible probability, $\sqrt{2}$ is unable to guarantee an 80% link reliability. Moreover, as K increases from the minimum one required for satisfying certain link reliability, network throughput tends to decrease, especially when link reliability requirement is high.

Our findings (in particular, those on the reliability-throughput tradeoff in ratio-K-based scheduling) suggest that, in wireless networked sensing and control where high link reliability is critical not only for reliable data delivery but also for small latency and latency jitter, we can use link reliability requirement as the basis of instantiating the ratio-K model. Accordingly, we propose the *physical-ratio-K (PRK) interference model* as a reliability-oriented instantiation of the ratio-K model, where the link-specific choice of K adapts to network and environmental conditions as well as application QoS requirements to ensure certain minimum reliability of every link.

To understand the potential effectiveness of PRK-based medium access control, we analyze the performance of PRK-based scheduling. We find that, for a given requirement on link reliability, PRK-based scheduling achieves a network spatial throughput very close to what is enabled by SINR-based scheduling, for instance, at least 95% in many scenarios we study. Moreover, as link reliability requirement increases, the throughput loss in PRK-based scheduling further decreases. Since link reliability is a locally measurable metric, reliability-oriented selection of K in PRK-based medium access control enables link-specific, local search of K via feedback on packet delivery reliability. This suggests new approaches to MAC protocol design in the presence of unpredictable traffic patterns, for instance, by letting the receiver of each link locally choose a K for satisfying application-specific link reliability requirement. This also addresses the challenge of how to efficiently adapt K according to dynamic, potentially unpredictable network and environmental settings, which has been recognized as an open problem by Shi $et\ al.$ [Shi et al. 2009] who studied the ratio-K model in parallel with our work.

The above analytical results give us insight into the behavior of ratio-K-based scheduling in uniform grid and random networks with a wide range of system configurations on factors such as traffic load, link length, and wireless signal attenuation. We have verified these insight through simulation as well as measurement study in both the NetEye and the MoteLab wireless sensor network testbeds which reflect real-world properties such as non-uniform network settings. As we will discuss in Section 4.2, even though the PRK model is conceived based on observations from the analysis of uniform network and environmental conditions, the locality of the PRK model and the existence of purely local procedures of adapting the PRK model parameter based on in-situ network and environmental conditions (as shown in our preliminary study [Zhang et al. 2012]) enable the PRK model to adapt to potentially heterogeneous conditions (e.g., in traffic load and wireless channel path loss) in different parts of a network, thus making the PRK model suitable for networks with heterogeneous conditions too.

The rest of the paper is organized as follows. In Section 2, we present the wireless channel and radio models used in the analytical part of this paper. We develop closed-form performance models of ratio-K-based scheduling in Section 3 and then study how system properties and optimization objectives affect the ratio-K model instantiation in Section 4. We also propose the PRK interference model in Section 4, and then we examine the optimality of PRK-based scheduling in Section 5. We corroborate our analytical results through testbed-based measurement and simulation in Sections 6 and 7, and we also examine similar issues for ultra-wideband (UWB) networks in Section 7. We discuss related work in Section 8 and make concluding remarks in Section 9. As a central point of reference, Table I summarizes the major notations used in the paper.

Notations first introduced in Sections 1 or 2	
$P(S_i, R_i)$	Strength of signals reaching the receiver R_i from the transmitter S_i
N_i	Background noise power at a receiver R_i
$D(S, R)$	Geographic distance from a node S to another node R
γ	Signal-to-interference-plus-noise-ratio (SINR) at a receiver
γ_0	Minimum SINR for satisfying a required link reliability (i.e., packet delivery rate)
K	The parameter of the ratio-K interference model
P_t	Transmission power
α	Wireless channel path loss exponent
BER	Bit error rate
PDR	Packet delivery rate
Notations first introduced in Sections 3 or 4	
L	An arbitrary link in the network
ℓ	Geometric length of link L in grid networks; average geometric link length in Poisson random networks.
$\ell'(L)$	Geometric length of link L; its mean is ℓ for both grid and random networks.
$\mathbb{ER}(L, K)$	Exclusion region of link L in ratio-K-based scheduling
$T_L(t)$	Throughput along a link L at time t
T_{net}	Network spatial throughput
$T_{net,grid}$	T_{net} in grid networks
$T_{net,Poisson}$	T_{net} in Poisson random networks
$q(t)$	Indicator function on whether there exist data packets queued for transmission along L at time t
β	Average probability that there exist data packets queued for transmission along L at any time instant
$tx(t)$	Indicator function on whether a transmission, if any, is successful at time t
I	Expected total interference at a receiver
λ	Node distribution density in Poisson random networks
λ_t	Density of the spatial distribution of concurrent transmitters in Poisson random networks
$K_{n_s,n_r,T_{pdr}}$	The parameter of the Physical-Ratio-K (PRK) interference model
$sd(T, R)$	$\frac{1}{P(T,R)}$, i.e., the *s-distance* from a node T to another node R, with $P(T, R)$ being the strength of signals reaching R from T.
Notations first introduced in Section 5	
γ_0'	Minimum SINR for satisfying a required ACK reliability
$\mathbb{S}_{prk}$, $\mathbb{S}_{sinr}$	Nodes in the exclusion region of link L in PRK- and SINR-based scheduling respectively
I_t, I_t'	Maximum tolerable interference at the receiver and the transmitter of link L respectively
I_{prk}, I_{sinr}	Actual interference at the receiver in PRK- and SINR-based scheduling respectively
I_{prk}', I_{sinr}'	Actual interference at the transmitter in PRK- and SINR-based scheduling respectively
T_{prk}, T_{sinr}	Network spatial throughput in PRK- and SINR-based scheduling respectively
T_{loss}	Throughput loss in PRK-based scheduling as compared with SINR-based scheduling
ΔX	Average number of nodes per exclusion region that are silenced in PRK-based scheduling but not in SINR-based scheduling

Table I: Major notations used in the paper

2. PRELIMINARIES

Here we present the wireless channel and radio models used in the analytical part of this paper.

Channel model. To characterize signal attenuation in wireless networks, we use the log-normal path loss model [Rappaport 2002] which is widely adopted in protocol design and analysis. By this model, the expected power $P(S, R)$ of the received signal at a node R that is of geographic distance $D(S, R)$ away from the transmitter S is computed as follows:

$$P(S, R) = \frac{P_t}{D(S, R)^\alpha}, \tag{1}$$

where P_t is the transmission power, α is the path loss exponent. In our study, we use different instantiations of α to represent different wireless environments.

Radio model. The reception capability of a radio can be characterized by the bit error rate (BER) and the packet delivery rate (PDR) in decoding signals with specific signal-to-interference-plus-noise-ratios (SINR). Focusing on wireless sensing and control networks, we base our study mainly on the commonly-used, IEEE 802.15.4-compatible CC2420 radios; we also study low-power UWB radios which are expected to be used for intra-vehicular sensing and control [Niu et al. 2008], and we present the results in Section 7. Based on the modulation and coding schemes of CC2420 radios, the BER for a packet reception is computed as follows [IEEE 802.15.4 2006]:

$$\text{BER}(\gamma) = \frac{8}{15} \times \frac{1}{16} \times \sum_{k=2}^{16} (-1)^k \binom{16}{k} e^{(20 \times \gamma \times (\frac{1}{k} - 1))}, \tag{2}$$

where γ is the signal-to-noise-plus-interference-ratio (SINR) for the received packet signal. Assuming independent bit errors as in existing analytical studies [Zuniga and Krishnamachari 2007], the PDR is computed as follows:

$$\text{PDR}(\gamma, f) = (1 - \text{BER}(\gamma))^{8f} \tag{3}$$

where γ is the SINR of the received packet signal, and f is the packet length (in units of bytes) including overhead such as packet header.

Remark. For analytical tractability, the aforementioned models do not capture all the real-world phenomena such as the irregularity in wireless communication [Zhou et al. 2006]. But the analysis based on these models gives us insight into wireless interference models, and the analytical results have also been verified through testbed-based measurement which captures complex real-world phenomena as we discuss in Section 6.

3. PERFORMANCE OF RATIO-K-BASED SCHEDULING

To explore effective methods of instantiating the ratio-K model, here we analyze network throughput and link reliability in ratio-K-based scheduling when the ratio-K model is instantiated with different Ks. Focusing on link-layer behavior, we consider the optimization objective of maximizing channel spatial reuse (i.e., maximizing the number of concurrent transmissions) in ratio-K-based scheduling. In this section and in Sections 4 and 5 accordingly, we mean, by network throughput, the network spatial throughput as defined by Equation (6); in our measurement study in Section 6, we consider end-to-end throughput which directly reflects network-wide behavior.

Towards characterizing the computational complexity of ratio-K-based scheduling in general, we first prove that the ratio-K-based scheduling is NP-hard as follows:[3]

PROPOSITION 3.1. *The problem of maximizing the number of interference-free concurrent transmissions is NP-hard when the interference model is the ratio-K model.* □

PROOF. We consider the case when $K > 1$, as is usually the case in practice. Then, the NP-hardness of ratio-K-based scheduling with maximum spatial reuse can be proved through a polynomial time reduction from the 3-CNF-SAT problem to ratio-K-based scheduling. The proof is the same as the proof for Theorem 2 of [Sharma et al. 2006] (which shows the NP-hardness of the Maximum Weighted K-Valid Matching problems) except for the following changes to the reduction:

— Instead of an abstract graph, the graph G is embedded onto a 2D plane where each node has a fixed location in the plane.
— For the subgraph corresponding to the s-th ($s = 1..m$) clause of the 3-CNF boolean formula, locate the nodes such that the links $(v^s_{i,f}, v^s_{i,b})(i = 1..3)$ are orthogonal to the links

[3]Even though the NP-hardness of K-hop-interference-model-based scheduling has been proved [Sharma et al. 2006], the NP-hardness of ratio-K-based scheduling has not been analyzed yet.

$(v^s_{i,f}, v^s_{i+1,f})(i = 1, 2)$ and that links $(v^s_{1,f}, v^s_{2,f})$ and $(v^s_{2,f}, v^s_{3,f})$ are along the same line. In addition, make the lengths of the links $(v^s_{i,f}, v^s_{i,b})(i = 1..3)$ and $(v^s_{i,f}, v^s_{i+1,f})(i = 1, 2)$ to be of one unit.

— Place all the subgraphs on the plane (e.g., in a big circle) such that every link connecting two subgraphs is at least $K(K > 1)$ units long.

Based on this new reduction method for constructing the graph G, the rest of the proof for Theorem 2 of [Sharma et al. 2006] is applicable to our proof here without any change. Due to the limitation of space, we skip the details here. □

We consider both grid and Poisson random networks in our analysis, but, given the NP-hardness of general ratio-K-based scheduling, we only consider the following special cases of the problem for computational tractability and for deriving closed-form formula for scheduling performance:

— To avoid the complication introduced by boundary effects in small, finite networks, we only consider infinite-sized networks so that the conditions (e.g., interference power) at any part of a network represent those of the rest of the network and that our analysis can focus on the conditions at any part of the network. (Note that infinite-sized networks also approximate large networks such as those envisioned for industrial control in large oil fields.)

— For grid networks, we only consider cases where the data transmission links are of equal length ℓ and ℓ is a multiple of grid hop length. We also assume a uniform traffic pattern where all the transmissions follow the same direction along the grid-line, which enables the maximum degree of spatial reuse in grid networks as we show in Appendix B. (Note that every node in the network is a potential transmitter.)

— For 2D Poisson random networks, we assume that nodes are distributed with an average density of λ nodes per unit area. The traffic pattern is such that the average link length is ℓ; each transmitter T sends packets to a receiver R such that the distance between T and R is the closest to ℓ, and if multiple such receivers exist, T randomly picks one as its receiver.

— For both grid and random networks, we assume that each transmitter has data packets buffered for transmission with an average probability β at any moment in time.[4]

The analytical results derived based on the above assumptions give us insight into the behavior of ratio-K-based scheduling in uniform grid and random networks with a wide range of system configurations on factors such as traffic load, link length, and wireless signal attenuation; the analytical insight will be verified in Sections 6 and 7 through testbed-based measurement and simulation where finite networks and non-uniform traffic patterns are considered without the above assumptions.

In data transmission scheduling, we consider both reliable reception of data at receivers and reliable reception of link-layer acknowledgments at transmitters. Let the length of a link L be ℓ, and T and R be the transmitter and receiver of L respectively. Then ratio-K-based scheduling defines two circular exclusion regions centered at T and R respectively, each with a radius $K\ell$, such that no other node in the exclusion regions can transmit concurrently with T. We regard the union of the transmitter- and receiver-side exclusion regions as the exclusion region of link L, and we denote it by $\mathbb{ER}(L, K)$. For instance, Figure 1 shows the exclusion region of link L in a grid network when K = 2. For convenience, we also use $\mathbb{ER}(L, K)$ to denote the set of nodes within the exclusion region, not including those on the boundary.

For the uniform network and traffic conditions considered in the analytical part of this paper (i.e., this section and Sections 4 and 5), the degree of channel spatial reuse is characterized by the size of exclusion regions, i.e., the number of nodes silenced by the transmission along a link L, and we denote it by $|\mathbb{ER}(L, K)|$. For link L, let BW be the radio transmission rate in terms of number of packets per unit time, $q(t)$ be the indicator function on whether there exist data packets queued for

[4] As we will discuss in Section 4.2 and corroborate via testbed-based measurement in Section 6, the PRK interference model to be formulated based on observations from the analysis of uniform network and environmental conditions is also applicable to networks with heterogeneous conditions such as heterogeneous traffic load.

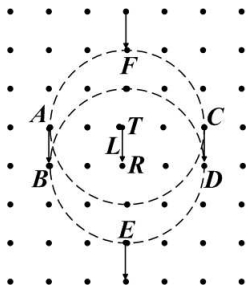

Figure 1: Scheduling based on the ratio-2 model in grid networks

transmission along L at time t, and $tx(t)$ be the indicator function on whether a transmission, if any, is successful at time t, then the number of packets successfully delivered along link L at time unit t is $BW \times q(t) \times tx(t)$. Considering the distance that successfully delivered packets travel (i.e., the length of link L) , we define the throughput along an arbitrary link L at time t, denoted by $T_L(t)$, as follows:

$$T_L(t) = (BW \times q(t) \times tx(t)) \times \ell'(L), \tag{4}$$

where $\ell'(L)$ is the length of link L, and the unit for $T_L(t)$ is "packet-distance-product per unit time". Then, the time average of $T_L(t)$ can be computed as

$$E_t[T_L(t)] = (BW \times E_t[q(t)] \times E_t[tx(t)]) \times \ell'(L) = (BW \times \beta \times \text{PDR}(L)) \times \ell'(L), \tag{5}$$

where β be the average probability that there exist data packets queued for transmission along L at any time instant, and PDR(L) is the packet delivery reliability over L. Accordingly, the network-wide link-layer throughput that considers both channel spatial reuse and per-link throughput can be characterized by[5]

$$T_{net} = E_{L,t}[\frac{T_L(t)}{|\mathbb{ER}(L,K)|}] = E_L[\frac{E_t[T_L(t)]}{|\mathbb{ER}(L,K)|}]. \tag{6}$$

Note that the unit for T_{net} is "packet-distance-product per unit time per node", and the definition of T_{net} is similar to the concept of *spatial throughput* which is commonly used in the literature of wireless network scheduling [Tabet and Knopp 2004]. T_{net} characterizes the average throughput from every node to its one-hop neighbors in the network; even though T_{net} only indirectly reflects the achievable multi-hop throughput, our testbed-based measurement study in Section 6 will show that the insight gained in the analysis applies to the case of multi-hop convergecast. Also note that T_{net} is of direct interest to the applications of inter-vehicle sensing and control, where one typical traffic pattern is single-hop communication between neighboring vehicles. For grid networks, $E_t[T_L(t)]$ and $|\mathbb{ER}(L,K)|$ are the same for all Ls, thus $T_{net,grid} = \frac{E_t[T_L(t)]}{|\mathbb{ER}(L,K)|}$. For Poisson random networks, $T_{net,Poisson} = E_L[\frac{E_t[T_L(t)]}{|\mathbb{ER}(L,K)|}] = \frac{BW \times \beta \times \ell \times E_L[PDR(L)]}{\lambda_t c}$, where λ_t and c are properties of the spatial distribution of concurrent transmitters in ratio-K-based scheduling for Poisson networks as we will discuss in Proposition 3.3 shortly.

Our objective is to study how the choice of K affects throughput T_{net} and link reliability PDR in ratio-K-based scheduling that maximizes channel spatial reuse. To compute T_{net}, the key is to compute the PDR along L. Using the radio model discussed in Section 2, we only need to derive

[5]We consider the expected value of $\frac{T_L(t)}{|\mathbb{ER}(L,K)|}$ to account for non-deterministic factors such as probabilistic packet transmissions over time and probabilistic node distribution over space in random networks. Focusing on link-layer behavior, this section and Sections 4 and 5 adopt this notion of network throughput; in our measurement study in Section 6, we consider end-to-end throughput which directly reflects network-wide behavior.

the SINR value at the receiver of L in order to compute the PDR. Since it is easy to compute the reception signal strength according to Equation 1, what remains is computing the interference at the receiver. In what follows, we present the method of computing receiver-side interference when transmissions are scheduled to maximize spatial reuse without violating the ratio-K model. In the analysis, we assume that the transmission power at each transmitter is P_t.

Grid networks. Given a specific parameter K, we analyze the spatial distribution of concurrent transmitters in ratio-K-based scheduling algorithms that maximize channel spatial reuse. Then we derive the interference incurred at a receiver according to the spatial distribution of concurrent transmitters. For $K = 2$, we have

PROPOSITION 3.2. *With ratio-2-based scheduling that maximizes channel spatial reuse, the expected total interference I at a receiver R in an infinite grid network is as follows:*

$$\begin{aligned} I \;=\; & P_t \times \beta \times \ell^{-\alpha} \times \\ & \Bigg(\textstyle\sum_{m=1}^{\infty} \big(\frac{2}{((2m)^2+1)^{\alpha/2}} + \frac{1}{(3m+1)^{\alpha/2}} + \frac{1}{(3m-1)^{\alpha/2}} \big) + \\ & \quad 2 \times \textstyle\sum_{m=1}^{\infty} \sum_{n=1}^{\infty} \left(\frac{1}{[(2m)^2+(3n+1)^2]^{\alpha/2}} + \frac{1}{[(2m)^2+(3n-1)^2]^{\alpha/2}} \right) \Bigg) \end{aligned} \tag{7}$$

where P_t is the transmission power, β is the node transmission probability, ℓ is the link length, and α is the wireless path loss exponent. I is finite as long as $\alpha > 2$. □

PROOF. To maximum channel spatial reuse, we need to generate the tightest tessellation of concurrent transmissions while conforming to the specification of the ratio-K interference model. For $K = 2$ and the transmission along an arbitrary link L as shown in Figure 1, six nodes (i.e., A - F) on the boundary of the exclusion region of L can be involved, either as a transmitter or a receiver, in concurrent transmissions. In a tightest tessellation of concurrent transmissions in ratio-2-based scheduling, this pattern of four concurrent transmissions/receptions around L applies to every other transmission in the network, thus we can derive the set $\mathcal{S}_i$ of concurrent transmitters that serve as interferers to the transmission along L.

If we define a coordinate system where the coordinates of R and T are $(0, 0)$ and $(0, \ell)$ respectively, then

$$\mathcal{S}_i = \{(2m\ell, (3n+1)\ell) : m \in \mathbb{Z}, n \in \mathbb{Z}, m^2 + n^2 \neq 0\} \tag{8}$$

where $\mathcal{S}_i$ is identified by the locations of the nodes in it, and $\mathbb{Z}$ is the set of all integers. In Figure 1, for instance, transmitter C's location is (2ℓ, ℓ) and the corresponding m and n are 1 and 0 respectively. The expected total interference I at the receiver R is the sum of the expected interference introduced by each concurrent transmitter n_i in $\mathcal{S}_i$. Based on the link model discussed in Section 2, we have

$$\begin{aligned} I \;&=\; \textstyle\sum_{n_i \in S_i} I_i \\ &=\; P_t \times \beta \times \textstyle\sum_{n_i \in S_i} d(n_i, R)^{-\alpha} \\ &=\; P_t \times \beta \times \ell^{-\alpha} \times \left(\textstyle\sum_m \sum_n \big(\frac{1}{[(2m)^2+(3n+1)^2]} \big)^{\alpha/2} \right) \end{aligned} \tag{9}$$

After some simple derivations, Equation 9 becomes Equation 7.

When $\alpha > 2$, the following holds:

$$\sum_{m=1}^{\infty} \frac{1}{((2m)^2+1)^{\alpha/2}} < \sum_{m=1}^{\infty} \frac{1}{m^{\alpha/2}}$$

The right hand side of the above inequality is a type of p-series where $p = \frac{\alpha}{2}$, and it converges when $p > 1$. Accordingly, $\sum_{m=1}^{\infty} \frac{1}{((2m)^2+1)^{\alpha/2}}$ converges when $\alpha > 2$. Using similar approach, we can prove that the other items of Equation 7 converges if $\alpha > 2$. Therefore, I converges and is finite as long as $\alpha > 2$. □

Note that, in grid networks, the total interference I is a function of link length ℓ but not the node distribution density (e.g., as characterized by the grid-hop length $\frac{\ell}{n}$ for some positive integer n).

Using Equation 7, we can compute the interference and thus the SINR at R, based on which we can compute link reliability and network throughput for the case of $K = 2$. Following approaches similar to the one for $K = 2$, we can derive the spatial distribution of concurrent transmitters and thus the receiver-side interference for cases when K takes other values. For conciseness of presentation, we refer readers to Appendix A for the detailed derivations.

Random networks. A random network where the number of nodes per unit area is a Poisson random variable with mean λ can be regarded as a stationary spatial Poisson process Φ with density λ [Stoyan et al. 1995]. Then the spatial distribution of concurrent transmitters in ratio-K-based scheduling can be modeled as a thinning spatial process that contains only a subset of the nodes in Φ (i.e., some nodes in Φ are thinned/silenced by transmissions from other nodes). For ratio-K-based scheduling that maximizes spatial reuse, in particular, the spatial distribution of concurrent transmitters can be modeled as a marked thinning process as follows [Stoyan et al. 1995; Baccelli and Blaszczyszyn 2010]:[6]

— We mark each node X of Φ with a random number $m(X)$ uniformly distributed over $(0, 1)$, and then we mark each link L with transmitter T and receiver R with a number $m(L) = \frac{m(T)+m(R)}{2}$;
— We define the links incident to a node X as the set of links whose transmitter or receiver is X, and we denote it by $\mathbb{L}(X)$; we also denote the link whose transmitter is X by $L(X)$. Then, the thinning process retains a transmitter $X \in \Phi$ if the mark of $L(X)$ is the smallest among those of all the links incident to some node within the exclusion region $\mathbb{ER}(L(X), K)$ of link $L(X)$. That is, the thinning process of concurrent transmitters is defined as follows:

$$\Phi_t = \{X \in \Phi : m(L(X)) < m(L), \forall L \in \cup_{Y \in \mathbb{ER}(L(X),K)} \mathbb{L}(Y)\} \tag{10}$$

The thinning process Φ_t as defined above can be approximated by a spatial Poisson process [Stoyan et al. 1995], and we derive its density λ_t as follows:

PROPOSITION 3.3. *The density λ_t of the thinning process Φ_t of concurrent transmitters computes as follows:*

$$\lambda_t = \frac{1 - exp(-\lambda c)}{c} \tag{11}$$

where $c = C(\ell, K)+(C(\ell, K+1)-C(\ell, K)) \int_0^\ell \frac{2arccos(\frac{\ell^2+\ell'^2+2K\ell\ell'}{2\ell(k\ell+\ell')})}{360\ell} d\ell'$, $C(\ell, K)$ and $C(\ell, K+1)$ is the area of the exclusion region $\mathbb{ER}(L, K)$ and $\mathbb{ER}(L, K + 1)$ of a ℓ-long link L respectively. □

PROOF. From the results in Section 5.4 of [Stoyan et al. 1995], the intensity λ_t of Φ_t is given by

$$\lambda_t = p_t \lambda$$

where p_t is the probability for a typical point of Φ to be retained in the thinning process Φ_t, and it is also called the *Palm retaining probability* in stochastic geometry [Stoyan et al. 1995]. As we will derive next, the retaining probability p_t computes as follows:

$$p_t = \int_0^1 r(t)dt = \frac{1 - exp(\lambda c)}{\lambda c} \tag{12}$$

where $c = C(\ell, K) + (C(\ell, K + 1) - C(\ell, K)) \int_0^\ell \frac{2arccos(\frac{\ell^2+\ell'^2+2K\ell\ell'}{2\ell(k\ell+\ell')})}{360\ell} \mathrm{d}\ell'$, and $r(t) = exp(-c\lambda t)$ is the probability for the thinning process Φ_t to retain a node T whose associated link $L(T)$ has mark t (i.e., $m(L(T)) = t$).

[6] This marked thinning process is an extension/variant of the basic Matern hard-core process, where each hard-core is a disk-area around a node such that only this node in the hard-core is retained in the thinning process, to cases where the hard-cores are the exclusion regions around links instead of circular disks [Stoyan et al. 1995].

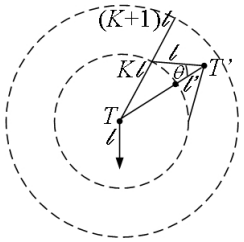

Figure 2: Probability that a transmitter $T' \in \mathbb{ER}(L, K+1) \setminus \mathbb{ER}(L, K)$ has its receiver in $\mathbb{ER}(L, K)$

The equation for $r(t)$ follows from the observation that the point process

$$\{X \in \Phi : m(X) < t\}$$

is a t-thinning of the Poisson process Φ, hence itself is a Poisson process of intensity λt. Therefore, $r(t)$ is the probability that an exclusion region $\mathbb{ER}(L, K+1)$ of a ℓ-long link contains no node who has an associated link with mark less than t, that is, containing no nodes of the t-thinning process.

In computing $r(t)$, the reason why c equals $C(\ell, K) + (C(\ell, K+1) - C(\ell, K)) \int_0^\ell \frac{2arccos(\frac{\ell^2+\ell'^2+2K\ell\ell'}{2\ell(k\ell+\ell')})}{360\ell} \mathrm{d}\ell'$ instead of $C(\ell, K)$ is because $\cup_{Y \in \mathbb{ER}(L(X),K)} \mathbb{L}(Y)$ may well contain links whose transmitter is in $\mathbb{ER}(L, K+1)$ but not in $\mathbb{ER}(L, K)$. For a transmitter $T' \in \mathbb{ER}(L, K+1) \setminus \mathbb{ER}(L, K)$ that is $K\ell + \ell'$ ($0 < \ell' \leq \ell$) from the transmitter T of link L as shown in Figure 2,

the probability that T' transmits to a node in $\mathbb{ER}(L, K)$ is $\frac{2\theta}{360}$ since the receiver of T' is at any direction around T' with equal probability. Since $(K\ell)^2 = \ell^2 + (K\ell + \ell')^2 - 2\ell(K\ell + \ell')cos\theta$, $\theta = arccos(\frac{\ell^2+\ell'^2+2K\ell\ell}{2\ell(K\ell+\ell')})$. Therefore, the probability that an arbitrary transmitter in $\mathbb{ER}(L, K+1) \setminus \mathbb{ER}(L, K)$ has its receiver in $\mathbb{ER}(L, K)$ is $\int_0^\ell \frac{2\alpha}{360} \frac{1}{\ell} \mathrm{d}\ell' \int_0^\ell \frac{2arccos(\frac{\ell^2+\ell'^2+2K\ell\ell'}{2\ell(k\ell+\ell')})}{360\ell} \mathrm{d}\ell'$, and the expected number of nodes in $\mathbb{ER}(L, K+1) \setminus \mathbb{ER}(L, K)$ whose receivers are in $\mathbb{ER}(L, K)$ is $\lambda(C(\ell, K+1) - C(\ell, K)) \int_0^\ell \frac{2arccos(\frac{\ell^2+\ell'^2+2K\ell\ell'}{2\ell(k\ell+\ell')})}{360\ell} \mathrm{d}\ell'$. Thus we have the formula for c. □

Then we can compute the total interference I at an arbitrary receiver R as follows:

PROPOSITION 3.4. *With ratio-K-based scheduling that maximizes channel spatial reuse, the expected total interference I at a receiver R in an infinite Poisson random network is as follows:*

$$I = \frac{2\pi\lambda_t P_t \beta}{(\alpha - 2)} (K\ell)^{2-\alpha} \tag{13}$$

where λ_t is given by Equation 11, P_t is the transmission power, β is the node transmission probability, α is the wireless path loss exponent, and ℓ is the link length. □

PROOF. Given that, in ratio-K-based scheduling that maximizes channel spatial reuse, the spatial distribution of concurrent transmitters is a spatial Poisson process, we leverage the existing results on the interference power in Poisson interference fields to derive the receiver-side interference in ratio-K-based scheduling. When the interferers are Poisson distributed with density λ and when each interferer transmits with probability one (i.e., $\beta = 1$), in particular, Weber et. al [Weber et al. 2005] have shown that, for an arbitrary receiver, the total interference from nodes more than r distance away from the receiver can be computed as follows:

$$m(\lambda) = \frac{2\pi\lambda P_t}{(\alpha - 2)} r^{2-\alpha}. \tag{14}$$

Accordingly, for an arbitrary transmission probability β, the total interference is

$$m(\lambda, \beta) = \frac{2\pi\lambda P_t \beta}{(\alpha - 2)} r^{2-\alpha}. \quad (15)$$

Based on the analysis earlier in this section, the set of concurrent transmitters in ratio-K-based scheduling that maximizes spatial reuse are Poisson distributed with density λ_t as shown in Equation 11. The concurrent transmitters are also more than $K\ell$ distance away from the receiver. Therefore, we can see from Equation 15 that the receiver-side interference I can be computed as follows:

$$I = m(\lambda_t, \beta) = \frac{2\pi\lambda_t P_t \beta}{(\alpha - 2)} (K\ell)^{2-\alpha}.$$

□

With the closed-form performance models of ratio-K-based scheduling developed in this section, we will examine in the next section the behavior of ratio-K-based scheduling in a wide range of network and environmental settings; based on the behavior of ratio-K-based scheduling, we will then propose the Physical-Ratio-K (PRK) interference model as the basis of instantiating the ratio-K model in interference-oriented wireless transmission scheduling.

4. THE PHYSICAL-RATIO-K (PRK) INTERFERENCE MODEL

Using the performance models of Section 3, we first numerically study how system properties and design objectives affect the effective instantiation of the ratio-K model, and then we propose the Physical-Ratio-K (PRK) interference model.

4.1. Numerical analysis of ratio-K-based scheduling

Using Equations 5 and 6, the CC2420 radio model described in Section 2, and the equations for computing interference (e.g., Equations 7 and 13), we numerically analyze the impact of parameter K on the network throughput and link reliability in ratio-K-based scheduling, and we analyze the impact that different network and environmental settings have on the effective choice of parameter K.

4.1.1. Methodology. To examine the impact of wireless attenuation in different environments, we consider the set $\{2.1, 2.6, 3, 3.3, 3.6, 3.8, 4, 4.5, 5\}$ of wireless path loss exponents αs, which represent a wide range of real-world environments [Sohrabi et al. 1999]. For the grid networks and Poisson random networks, we vary their parameters such as traffic load, link length, and node distribution density to examine the impact of network properties. Traffic load is controlled by the transmission probability β, and we consider the set $\{0.05, 0.1, 0.15, \ldots, 1\}$ of βs. Link length is chosen so that the link reliability varies from 1% to 100% in the absence of interference. More specifically, for each specific path loss exponent α, we choose a link length ℓ_0 corresponding to an interference-free packet delivery rate (PDR) of 1%, and another link length ℓ_1 corresponding to a signal-to-noise-ratio (SNR) of 5dB more than the minimum SNR for ensuring 100% interference-free PDR; then we take 60 sample link lengths that are uniformly distributed between ℓ_0 and ℓ_1. (Note that the transmission power level is set at -25dBm in our study.) For each average link length ℓ in random networks, we select a set of node distribution densities λs so that the average number of nodes in a circular area of radius ℓ is 5, 10, 15, 20, 30, and 40 respectively.

For convenience, we regard each setting of network and environment parameters as a *system configuration* hereafter. Thus our study examines 75,600 different system configurations, and the boxplots, medians, and distributions to be presented in the rest of the paper are mostly based on the distribution of the corresponding metrics across different system configurations. For each system configuration, we analyze the network performance when the ratio-K model is instantiated with different Ks. The set of Ks we consider are $\{\sqrt{2}, 2, \sqrt{5}, \sqrt{8}, 3, \sqrt{10}, \sqrt{13}, 4, \sqrt{18}, \sqrt{20}, 5, \sqrt{26},$

Common to grid and Poisson random networks	
α	$\{2.1, 2.6, 3, 3.3, 3.6, 3.8, 4, 4.5, 5\}$
β	$\{0.05, 0.1, 0.15, \ldots, 1\}$
ℓ	For each α, take 60 sample link lengths that are uniformly distributed between link lengths ℓ_0 and ℓ_1, with the link length ℓ_0 corresponding to an interference-free packet delivery rate (PDR) of 1% and the link length ℓ_1 corresponding to a signal-to-noise-ratio (SNR) of 5dB more than the minimum SNR for ensuring 100% interference-free PDR.
For grid networks only	
K	$\{\sqrt{2}, 2, \sqrt{5}, \sqrt{8}, 3, \sqrt{10}, \sqrt{13}, 4, \sqrt{18}, \sqrt{20}, 5, \sqrt{26}, \sqrt{29}, \sqrt{34}, 6\}$
For Poisson random networks only	
λ	For each average link length ℓ, select a set of node distribution densities λs so that the average number of nodes in a circular area of radius ℓ is 5, 10, 15, 20, 30, and 40 respectively.
K	$\{1, 1.5, 2, 2.5, \ldots, 10\}$

Table II: Parameter settings for numerical analysis

$\sqrt{29}$, $\sqrt{34}$, $6\}$[7] for grid networks, and $\{1, 1.5, 2, 2.5, \ldots, 10\}$ for Poisson random networks. As a quick reference, Table II summarizes the parameter settings used in the numerical analysis.

Using the numerical results on network throughput and link reliability in the 75,600 system configurations, we analyze 1) the impact of different factors on the best ratio-K model instantiation, 2) the sensitivity of model instantiation, and 3) the tradeoff between reliability and throughput in instantiating the ratio-K model. *The observations in grid networks and random networks are similar, thus here we only present results for grid networks; detailed results for random networks can be found in our technical report [Zhang et al. 2012].*

4.1.2. Sensitivity of ratio-K-based scheduling. We have analyzed how different network and environmental factors affect the optimal K that maximizes network throughput and the minimum K for ensuring certain link packet delivery rate (PDR). We have found that network and environmental properties significantly affect the best instantiation of the ratio-K model. Due to the limitation of space, we relegate the detailed discussion to our technical report [Zhang et al. 2012]; but to illustrate the drawbacks of choosing a constant K for ratio-K-based scheduling as in most existing study, we present in what follows the summary results on the sensitivity of network throughput and link reliability with respect to network and environmental dynamics.

Throughput. Given that the optimal K for maximizing network throughput changes with network and environmental properties, using any constant K in ratio-K-based scheduling may lead to throughput loss since the chosen K may not always be optimal. To quantify the impact of not adapting K to network and environmental dynamics, we compute, for each system configuration, the loss in network throughput when using a K that is ΔK away from the optimal K, denoted by K_{opt}, for this system configuration.[8] For different ΔK's, Figure 3 shows the boxplot[9] of throughput loss across different system configurations, where the loss is defined as the reduction in throughput divided by the optimal throughput. We see that, in general, throughput loss increases as $|\Delta K|$ increases. If the used K differs from the optimal one by up to 1, throughput loss can be up to 68%, which is non-negligible.

[7] These Ks are chosen in a *continuous* manner in the sense that, given a receiver, the inner area enclosed by the boundaries of the exclusion regions associated with every two closest Ks does not contain any node.We find that, for ratio-K-based scheduling in grid networks, increasing K after K is already greater than 5 can only increase link reliability but not network throughput. Thus 6 is large enough to serve as the largest K in our study.

[8] For each system configuration, we compute the network spatial throughput when different Ks are used. Then we set K_{opt} as the K whose corresponding network throughput is the largest.

[9] Note that, for clarity of presentation, we group data by the rounded ΔK instead of ΔK directly because there are too many ΔK's to present individually in a single figure.

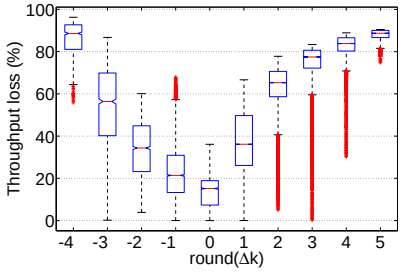

Figure 3: Throughput loss when using $K = K_{opt} + \Delta K$ for the ratio-K model, where K_{opt} is the optimal K for maximizing throughput in a system configuration. ΔK is rounded for clarity of presentation.

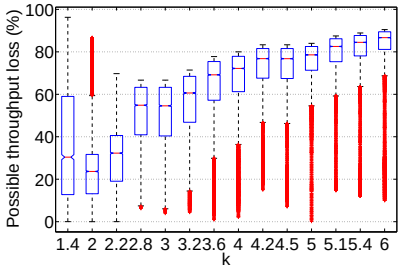

Figure 4: Possible throughput loss by choosing a constant K

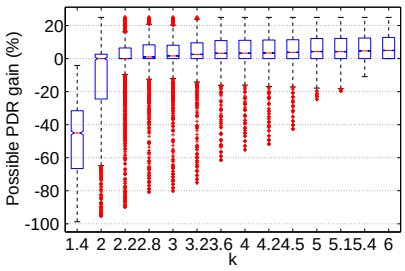

Figure 5: Impact of using a constant K: PDR req. = 80%

To understand the impact of choosing a fixed K, Figure 4 shows, for different fixed Ks, the possible throughput loss across different system configurations. We see that the throughput loss can be significant. For instance, fixing K to 2 can lead to a throughput loss of up to 86.73% and a median loss of 23.68%.

Therefore, *using a constant K across different network and environmental settings may well lead to significant loss in network throughput*, and, to avoid biased evaluation against ratio-K-based scheduling, we need to take this into account in both protocol design and performance analysis.

Reliability. To understand the impact of using a constant K on link reliability, we consider system configurations where a proper choice of K can ensure a link reliability of at least 20%, 40%, 60%, 80%, and 100%. Due to the limitation of space, here we only present the data for configurations where a link reliability of at least 80% can be achieved by choosing a proper K. (Similar phenomena as what we will present have been observed for other configurations too.) Figure 5 shows, for using different Ks, the boxplot of the PDR (i.e., packet delivery rate) gain across different system configurations, where the PDR gain is defined as $\frac{\text{PDR}_k - 0.8}{0.8}$ and PDR_k is the PDR resulting from using a specific constant K in a system configuration.

We see that *values of K less than or equal to 2 tend not to be a good constant number for ensuring reliable data delivery* (e.g., 80% link PDR): a constant K of 2 is unable to guarantee 80% link reliability with non-negligible probability; a constant K of $\sqrt{2}$ is mostly unlikely to guarantee 80% reliability, even though $\sqrt{2}$ is the optimal K for maximizing throughput in a wide variety of system configurations we study. On the other hand, *using larger Ks (e.g., 4) can improve link reliability, but this usually comes at the cost of reduced network throughput* due to reduced spatial

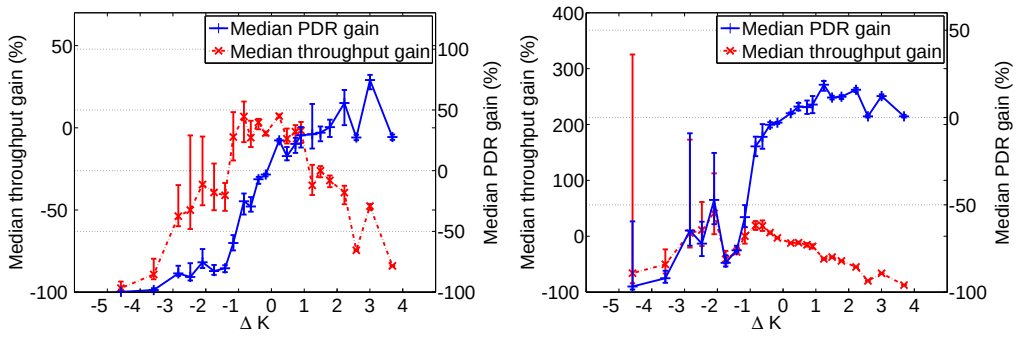

(a) PDR req. = 40%

(b) PDR req. = 80%

Figure 6: Δk vs. performance gain

reuse of channel resources (as can be seen from Figure 4). We study this tradeoff between reliability and throughput in detail next.

4.1.3. Tradeoff between reliability and throughput. The above discussion has alluded to the inherent tradeoff between link reliability and network throughput in instantiating the ratio-K model. In what follows, we examine the issue in detail. We numerically study the tradeoff because it is difficult to derive the closed-form formula for the relationship between link reliability and network throughput in general. For each link reliability requirement (e.g., 80%) and each system configuration that can ensure the reliability by using certain minimum $K = K_0$, we compute the performance gain in packet delivery rate (PDR) and throughput when changing K to $K' = (K_0 + \Delta K)$ for various ΔK's. The performance gain is defined as $\frac{X_{K'} - X_0}{X_0}$, where X_0 is the PDR (or throughput) when $K = K_0$ and $X_{K'}$ is the PDR (or throughput) when $K = K'$.

Figure 6 shows the median performance gains for system configurations where a certain minimum PDR can be ensured. We observe the following:

— Maximum network throughput is usually not achieved at the minimum K for ensuring certain a link reliability but at a smaller K; (This is because smaller Ks increase channel spatial reuse.)
— As K increases from the minimum one for ensuring certain link reliability, network throughput tends to decrease with high probability even though link reliability does improve; (This is because increasing K reduces channel spatial reuse.)
— As PDR requirement increases, moreover, the probability of improving throughput by increasing K from the minimum one of ensuring the PDR requirement further decreases, in addition to being small all the time. (This is because a higher PDR requirement implies a larger minimum K for ensuring the required PDR and thus less channel spatial reuse already; further increasing K leads to further reduction in channel spatial reuse and thus the reduction in network spatial throughput with higher probability.)

Implications. These findings suggest that we should use, in protocol design, the minimum K that ensures the required link reliability, since this helps avoid throughput reduction (e.g., due to the use of unnecessarily large Ks) while ensuring enough reliability at the same time. In general, the minimum link reliability required is application dependent, and it relates to the question of how to balance properties such as throughput, reliability, delay, and energy efficiency. In low-power wireless sensing and control networks such as those for industrial sensing and control, however, it is usually desirable to have high link reliability for the following reasons: 1) reliable data delivery itself is usually important for mission-critical sensing and control; 2) higher reliability implies less

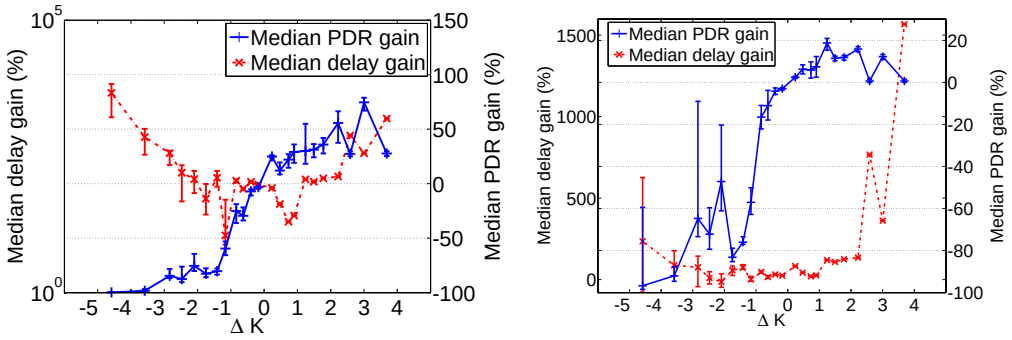

(a) PDR req. = 40%

(b) PDR req. = 80%

Figure 7: Δk vs. delay increase: TDMA

variability and better predictability in data delivery performance (e.g., timeliness); this is because, given a link reliability p, the coefficient-of-variation of packet transmission status (i.e., success or failure) is $\sqrt{\frac{1-p}{p}}$ which decreases as p increases; 3) higher reliability implies fewer number of packet retransmissions and thus less energy consumption. Given that, for high reliability requirement, the probability of throughput loss is high when we increase K beyond the minimum one required for ensuring reliability, PDR requirement can serve as a good basis for a node to choose the right K to use.

Choosing the minimum K that ensures the required link reliability also tends to help reduce data delivery delay. For grid networks with TDMA channel access control, for instance, Figure 7 shows the highly-likely increase in one-hop data delivery delay as K deviates, by ΔK, from the minimum one K_0 that ensures a required link reliability. (Interested readers can find the delay analysis in Appendix C.) As K increases from K_0, the delay increases because the number of nodes in a link's exclusion region increases, which introduces larger contention delay in channel access. As K decreases from K_0, the contention delay decreases, but the overall delay still tends to increase because retransmissions are required to ensure the same link-layer data delivery reliability as what is enabled by K_0 without retransmission. Similar phenomena are observed for random networks and contention-based channel access control mechanisms (see Appendix C).Given that the performance (e.g., convergence rate) of networked control usually decreases dramatically with increasing network delay, it is important to ensure small network delay in mission-critical sensing and control, which further emphasizes the need for high link reliability.

4.2. The PRK interference model

Summary of ratio-K-based scheduling. Through the above detailed study with different configurations of grid and random networks, we find that both network throughput and link reliability are sensitive to the choice of K in instantiating the ratio-K model. Thus it is important to take this into account in protocol design, for instance, by adapting K to network and environmental dynamics. We also observe that there is inherent tradeoff between link reliability and network throughput. In ratio-K-based scheduling, therefore, it is desirable to use the minimum K that ensures the required link reliability, since this tends to avoid throughput loss caused by using any unnecessarily large K. This observation suggests that link reliability requirement can serve as a good basis for each node to choose the right K to use in ratio-K-based scheduling.

PRK interference model. Based on the above observations on the behavior of ratio-K-based scheduling, we propose the *physical-ratio-K* (PRK) interference model as a link-reliability-based

instantiation of the ratio-K model as follows: "Given a transmission from node n_s to node n_r, a concurrent transmitter n_i does not interfere with the reception at n_r if and only if the following holds:

$$P(n_i, n_r) < \frac{P(n_s, n_r)}{K_{n_s,n_r,T_{pdr}}} \tag{16}$$

where $P(n_i, n_r)$ and $P(n_s, n_r)$ is the strength of signals reaching n_r from n_i and n_s respectively, and $K_{n_s,n_r,T_{pdr}}$ is chosen such that the probability of n_r successfully receiving packets from n_s is at least T_{pdr} in the presence of interference from all concurrent transmitters." It is usually difficult to derive closed-form formula for computing the parameter $K_{n_s,n_r,T_{pdr}}$ in general. But $K_{n_s,n_r,T_{pdr}}$ is amenable to online, distributed instantiation, because link reliability is a locally measurable metric and can even be identified through real-time, data-driven, passive measurement [Zhang et al. 2009]. In particular, the problem of identifying parameter $K_{n_s,n_r,T_{pdr}}$ can be modeled as a classical *regulation control* problem [Hellerstein et al. 2004], where the "reference input" is the required link reliability T_{pdr}, the "control input" is the parameter $K_{n_s,n_r,T_{pdr}}$, and the "feedback" is the current link reliability from n_s to n_r. That is, given a "reference input" of the required link reliability T_{pdr}, the receiver n_r can adapt the "control input" of $K_{n_s,n_r,T_{pdr}}$ so that the actual link reliability from n_s to n_r converges to T_{pdr}, where the adaptation of $K_{n_s,n_r,T_{pdr}}$ can be based on feedback control theory [Hellerstein et al. 2004]. Our preliminary study [Zhang et al. 2012] shows that this control-theoretic approach to instantiating the PRK model parameter $K_{n_s,n_r,T_{pdr}}$ is quite promising; through purely local adaptation, for instance, the distributed controllers converge to a state where the desired link reliability is guaranteed for each link while ensuring close-to-optimal concurrency in scheduling. Because the adaptation of K is local and the signal strength between nearby nodes is a pairwise, locally measurable metric too, we expect the PRK model to be a good basis for designing distributed scheduling/MAC protocols. Since our focus in this paper is understanding the behavior of ratio-K-based scheduling instead of protocol design, we relegate the design of distributed, PRK-based scheduling protocols to our future work. But we will study the potential performance of PRK-based scheduling in Section 5.

Based on the above discussion, we see that the PRK model has the locality of the ratio-K model. The PRK model also has the high fidelity of the SINR model, since it is based on link reliability which captures the properties and constraints of wireless communication. Even though the parameter $K_{n_s,n_r,T_{pdr}}$ of the PRK model depends on interference from all concurrent transmitters in the network as in the SINR model, the PRK model is simpler than the SINR model in terms of distributed protocol design. This is because, unlike the SINR model which *explicitly* characterizes interference from each concurrent transmitter in the whole network, interference is modeled *implicitly* in the PRK model through locally measurable link reliability without worrying about who the concurrent transmitters are. Thus, the PRK model enables a receiver to locally adapt the parameter K for satisfying its local link reliability requirement without explicit network-wide coordination. Note that the link-reliability-based definition of the PRK model also implicitly reflects many network and environmental factors such as network topology, traffic pattern, and wireless channel path loss, since the impact of these factors on interference control is reflected in the resulting link reliability. Also note that, even though the PRK model is conceived based on observations from the analysis of uniform network and environmental conditions, the locality of the PRK model and the existence of purely local procedures of adapting the PRK model parameter based on in-situ network and environmental conditions (as shown in our preliminary study [Zhang et al. 2012]) enable the PRK model to adapt to potentially heterogeneous conditions (e.g., in traffic load and wireless channel path loss) in different parts of a network, thus making the PRK model suitable for networks with heterogeneous conditions too; the applicability of the PRK model in heterogeneous network and environmental conditions will also be corroborated via testbed-based measurement in Section 6.

We define the PRK model based on signal strength instead of geographic distance so that the model is more generically applicable, for instance, to scenarios where transmission power varies across nodes [Moscibroda et al. 2006] or signal attenuation is non-uniform such as in our measure-

ment study of Section 6. Signal-strength-based definition of the PRK model also makes it readily applicable to field implementation since the precise distance between two nodes is difficult to estimate in real-world settings in general. Note that the selection of $K_{n_s,n_r,T_{pdr}}$ is based on each link of a receiver n_r such that the model can also be applied to cases where different links of a receiver vary significantly, for instance, in their senders' transmission powers.

To relate the PRK model to the ratio-K model and to facilitate discussions in Sections 5 and 6, we define the concept *s-distance* as follows: the s-distance from a node T to another node R, denoted by $sd(T,R)$, is $\frac{1}{P(T,R)}$ where $P(T,R)$ is the strength of signals reaching R from T. If $sd(T_1,R) > sd(T_2,R)$, then T_1 is regarded as *s-farther* away from R than T_2 is, and T_2 is regarded as *s-closer* to R than T_1 is. Given a $K_0 = K_{n_s,n_r,T_{pdr}}$, the PRK model defines an exclusion region $\mathbb{ER}(n_r,K_0)$ around the receiver n_r such that a node n_j is in $\mathbb{ER}(n_r,K_0)$ if and only if $sd(n_j,n_r) < \mathbb{R}(n_s,n_r,K_0)$, where $\mathbb{R}(n_s,n_r,K_0) = \frac{K_0}{P(n_s,n_r)}$ is called the *s-radius* of the exclusion region $\mathbb{ER}(n_r,K_0)$.

5. OPTIMALITY OF PRK-BASED SCHEDULING

While detailed study of distributed protocol design using the PRK model is a part of our future work, we analyze in this section the optimality of PRK-based scheduling as compared with SINR-based scheduling to gain insight into the potential effectiveness of PRK-based scheduling.[10] For ensuring data delivery reliability in wireless networked sensing and control, we conduct our comparative analysis on the condition that the link reliability in PRK- and SINR-based scheduling be the same.

5.1. Throughput loss in PRK-based scheduling

Similar to Sections 3 and 4, our analysis here considers infinite-sized grid and Poisson random networks with uniform traffic patterns; we will verify the analytical insight in Sections 6 and 7 through testbed-based measurement and simulation where finite networks and non-uniform traffic patterns are considered. We consider the scheduling algorithms that maximize channel spatial reuse while ensuring the required link reliability; in particular, given a link L, the scheduling algorithms try to find a maximum set of concurrent transmitters whose transmissions can occur in parallel with the transmission along link L while ensuring the required link reliability.

To satisfy a certain link reliability requirement and thus a certain packet-delivery-rate (PDR) for data and acknowledgment (ACK) reception along a link L, we need to make sure that the SINR at the receiver R and the transmitter T is above a certain threshold γ_0 and γ_0' respectively. For a given received signal strength P_r and background noise N_0 at R, this requirement translates into a requirement on controlling the maximum interference I_t at R to be $\frac{P_r}{\gamma_0} - N_0$. Similarly, we can derive the maximum tolerable interference I_t' at T.[11] To control interference, we need to silence the transmission of some nodes in the network, and, to maximize channel spatial reuse (i.e., maximizing the number of concurrent transmitters), we need to minimize the number of silenced transmitters. To this end, we have

PROPOSITION 5.1. *Silencing nodes s-closer to R (or T) rather than those s-farther away can minimize the number of nodes silenced for ensuring certain minimum SINR at the receiver R (or the transmitter T) in both PRK- and SINR-based scheduling that maximizes channel spatial reuse while ensuring the required link reliability.* □

PROOF. The PRK model requires silencing all the nodes within an exclusion region around the receiver (or the transmitter), and a node s-closer to the receiver (or the transmitter) has to be silenced

[10] Here we do not perform detailed comparative study between PRK- and ratio-K-based scheduling because it is obvious from Section 4 that, by adapting to network and environmental conditions as well as application requirements, PRK-based scheduling will perform better than ratio-K-based scheduling.

[11] I_t' may or may not equal to I_t depending on the ACK mechanism and the wireless radios. Accordingly, the exclusion regions around the sender and the receiver of a transmission may or may not be the same in PRK-based scheduling.

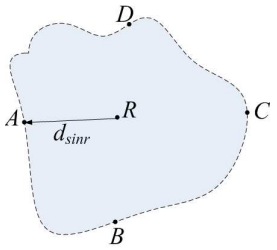

Figure 8: Difference in PRK- and SINR-based scheduling: receiver oriented view

if any node s-farther away from the receiver (or the transmitter) is silenced. Thus the proposition holds for PRK-based scheduling.

For SINR-based scheduling, we prove the proposition by contradiction. Suppose the receiver R has two potential interferers A and B nearby. The s-distances from A and B to receiver R are d_A and d_B respectively, with $d_A < d_B$. Assume, by contradiction, that silencing B instead of A would reduce the number of silenced nodes to ensure the required SINR at R. The fact is, however, that the interference that node A, if not silenced, generates is greater than that generated by B. To ensure that the total interference incurred to R does not exceed the threshold I_t, therefore, the number of nodes that have to be silenced when B but not A is silenced is no less than the number of nodes that have to be silenced when A but not B is silenced. Thus, silencing B instead of A does not reduce the number of silenced nodes. The same argument applies to the transmitter T. Thus the proposition holds for the SINR-based scheduling. □

Proposition 5.1 implies that, in scheduling algorithms that maximize channel spatial reuse, the set $\mathcal{S}$ of nodes silenced by the data reception at receiver R are the $|\mathcal{S}|$ number of nodes s-closest to R, where $|\mathcal{S}|$ denotes the cardinality of the set $\mathcal{S}$. We denote the set of nodes silenced by R in SINR- and PRK-based scheduling as $\mathcal{S}_{sinr}$ and $\mathcal{S}_{prk}$ respectively. For a tolerable interference I_t at R, we let I_{sinr} and I_{prk} be the actual interference incurred at R in SINR- and PRK-based scheduling respectively. Similarly, for correct ACK reception at the transmitter T in SINR- and PRK-based scheduling, we denote the set of silenced nodes as $\mathcal{S}'_{sinr}$ and $\mathcal{S}'_{prk}$ respectively, and, for a tolerable interference I'_t at T, we let I'_{sinr} and I'_{prk} be the actual interference incurred at T respectively. We also define $\mathbb{S}_{sinr} = \mathcal{S}_{sinr} \cup \mathcal{S}'_{sinr}$ and $\mathbb{S}_{prk} = \mathcal{S}_{prk} \cup \mathcal{S}'_{prk}$ to represent the set of silenced nodes around link L in SINR- and PRK-based scheduling respectively. Then,

PROPOSITION 5.2. *Given the tolerable interference I_t and I'_t at the receiver R and the transmitter T respectively, $\mathbb{S}_{sinr} \subseteq \mathbb{S}_{prk}$, $I_{prk} \leq I_{sinr} \leq I_t$, and $I'_{prk} \leq I'_{sinr} \leq I'_t$.* □

PROOF. Let the longest s-distance from a node in $\mathcal{S}_{sinr}$ to R be d_{sinr}. By the definition of the PRK and the SINR models and Proposition 5.1, all the nodes in $\mathcal{S}_{sinr}$ and $\mathcal{S}_{prk}$ are within d_{sinr} s-distance away from the receiver R. The difference between the PRK model and the SINR model is that, by the definition of the PRK model (see Inequality 16), all the nodes that are d_{sinr} s-distance away from R have to be silenced in the PRK model as long as at least one of them has to be silenced; whereas in the SINR model, we only need to silence the minimum number of nodes d_{sinr} s-distance away from R to ensure that the SINR at R is at least γ_0. For example, in Figure 8, there are four nodes d_{sinr} s-distance away from R. While the SINR model may only need to silence node A to guarantee the SINR threshold I_t, the PRK model will silence all the four nodes d_{sinr} away. Therefore, $\mathcal{S}_{sinr} \subseteq \mathcal{S}_{prk}$. Since $\mathcal{S}_{sinr} \subseteq \mathcal{S}_{prk}$, $I_{prk} \leq I_{sinr}$. SINR-based scheduling will ensure that $I_{sinr} \leq I_t$. Thus, $I_{prk} \leq I_{sinr} \leq I_t$ holds.

Similar argument applies to the transmitter T. Thus, $\mathcal{S}'_{sinr} \subseteq \mathcal{S}'_{prk}$, and $I'_{prk} \leq I'_{sinr} \leq I'_t$. Since $\mathcal{S}_{sinr} \subseteq \mathcal{S}_{prk}$ and $\mathcal{S}'_{sinr} \subseteq \mathcal{S}'_{prk}$, $\mathbb{S}_{sinr} \subseteq \mathbb{S}_{prk}$. □

Now, we are ready to derive the upper bound on the throughput loss in PRK-based scheduling as compared with SINR-based scheduling. By Equations 6 and 5, the throughput of PRK- and SINR-based scheduling, denoted by T_{prk} and T_{sinr} respectively, can be computed as follows:

$$T_{prk} = \frac{T_{R,prk}}{|\mathbb{S}_{prk}|}, \quad T_{sinr} = \frac{T_{R,sinr}}{|\mathbb{S}_{sinr}|}$$

where $T_{R,prk}$ and $T_{R,sinr}$ are the link throughput to R in PRK- and SINR-based scheduling respectively. From Proposition 5.2, we know that the average link reliability in SINR-based scheduling is no higher than that in PRK-based scheduling (since the actual interference incurred in SINR-based scheduling is no less than that in PRK-based scheduling). Thus, $T_{R,sinr} \leq T_{R,prk}$. Then, we can define the throughput loss T_{loss} in PRK-based scheduling as

$$T_{loss} = \frac{T_{sinr} - T_{prk}}{T_{sinr}} = \frac{\frac{T_{R,sinr}}{|\mathbb{S}_{sinr}|} - \frac{T_{R,prk}}{|\mathbb{S}_{prk}|}}{\frac{T_{R,sinr}}{|\mathbb{S}_{sinr}|}} \leq \frac{\frac{T_{R,sinr}}{|\mathbb{S}_{sinr}|} - \frac{T_{R,sinr}}{|\mathbb{S}_{prk}|}}{\frac{T_{R,sinr}}{|\mathbb{S}_{sinr}|}} = \frac{|\mathbb{S}_{prk}| - |\mathbb{S}_{sinr}|}{|\mathbb{S}_{prk}|} \quad (17)$$

Let n_b be the node in $\mathcal{S}_{sinr}$ that is s-farthest away from the receiver R, P_0 be the power of signals that reach R from n_b, and N_b be the number of nodes in the network whose s-distance to R is $sd(n_b, R)$. Similarly, let n'_b be the node in $\mathcal{S}'_{sinr}$ that is s-farthest away from the transmitter T, P'_0 be the power of signals that reach T from n'_b, and N'_b be the number of nodes whose s-distance to T is $sd(n'_b, T)$. Then,

PROPOSITION 5.3. *The expected T_{loss} is less than or equal to* $\frac{1}{|\mathbb{S}_{prk}|}(\min\{\frac{I_t - I_{prk}}{P_0 \times \beta}, N_b\} + \min\{\frac{I'_t - I'_{prk}}{P'_0 \times \beta}, N'_b\})$. □

PROOF. Let $dist(n_b, R)$ be the s-distance from n_b to R, and $dist(n'_b, T)$ be the s-distance from n'_b to T. Then from the proof of Proposition 5.2, we know that the s-distance d from every node in $\mathcal{S}_{prk} \setminus \mathcal{S}_{sinr}$ to R is $dist(n_b, R)$ since the PRK model silences all the nodes on the boundary of the exclusion region around R. Similarly, the s-distance d' from every node in $\mathcal{S}'_{prk} \setminus \mathcal{S}'_{sinr}$ to T is $dist(n'_b, T)$.

Given the interference tolerance I_t and I'_t at R and T respectively, the set of silenced nodes $\mathbb{S}_{prk}$ is fixed for a tightest tessellation of concurrent transmitters in a specific network and environmental setting. To understand the upper bound on T_{loss}, we need to understand the upper bound on $(|\mathbb{S}_{prk}| - |\mathbb{S}_{sinr}|)$ (*see* Inequality 17). By the definition of $\mathbb{S}_{prk}$ and $\mathbb{S}_{sinr}$, we know that $|\mathbb{S}_{prk}| - |\mathbb{S}_{sinr}| \leq (|\mathcal{S}_{prk}| - |\mathcal{S}_{sinr}|) + (|\mathcal{S}'_{prk}| - |\mathcal{S}'_{sinr}|)$. To upper bound $(|\mathbb{S}_{prk}| - |\mathbb{S}_{sinr}|)$, we analyze in what follows the upper bound on $(|\mathcal{S}_{prk}| - |\mathcal{S}_{sinr}|)$ and $(|\mathcal{S}'_{prk}| - |\mathcal{S}'_{sinr}|)$.

We first derive the upper bound on $(|\mathcal{S}_{prk}| - |\mathcal{S}_{sinr}|)$. Since all the nodes in $\mathcal{S}_{prk} \setminus \mathcal{S}_{sinr}$ are on the boundary of the exclusion region around R and are $dist(n_b, R)$ s-distance away from R, each such node introduces an expected interference of $P_0 \times \beta$ at receiver R. To ensure that the expected interference at R is no more than I_t (a.k.a., the SINR at R is above γ_0), one necessary condition is that the expected interference introduced by nodes in $\mathcal{S}_{prk} \setminus \mathcal{S}_{sinr}$ should be no more than $I_t - I_{prk}$, that is, the number of nodes in $\mathcal{S}_{prk} \setminus \mathcal{S}_{sinr}$ should be no more than $\frac{I_t - I_{prk}}{P_0 \times \beta}$. Note that this upper bound is usually not tight and not a sufficient condition because the interference at R tends to exceed I_t if the interference from nodes in $\mathcal{S}_{prk} \setminus \mathcal{S}_{sinr}$ reaches $I_t - I_{prk}$. This is because, if we add, for every area of the same size of the exclusion region around R, $\frac{I_t - I_{prk}}{P_0 \times \beta}$ more transmitters on average in SINR-based scheduling than in PRK-based scheduling, the interference at R will exceed $I_t - I_{prk}$ when the area covered by the network is larger than the exclusion region around R (which is usually the case). Therefore, an upper bound on the number of nodes in $\mathcal{S}_{prk} \setminus \mathcal{S}_{sinr}$ is $\frac{I_t - I_{prk}}{P_0 \times \beta}$. In addition, the number of nodes on the boundary of the exclusion region around R is no more than N_b, thus $(|\mathcal{S}_{prk}| - |\mathcal{S}_{sinr}|) \leq \min\{\frac{I_t - I_{prk}}{P_0 \times \beta}, N_b\}$.

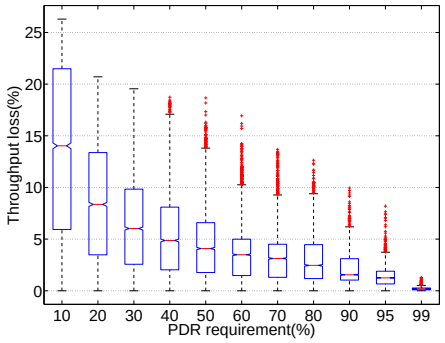

Figure 9: Throughput loss in PRK-based scheduling

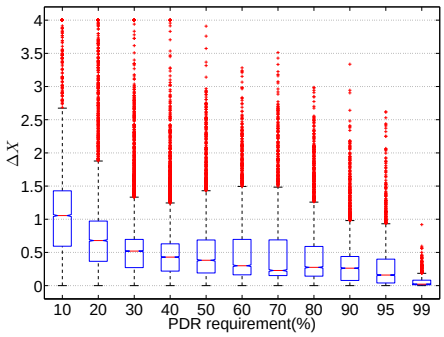

Figure 10: ΔX

Similarly, we can derive that $(|\mathcal{S}'_{prk}| - |\mathcal{S}'_{sinr}|) \leq \min\{\frac{I'_t - I'_{prk}}{P'_0 \times \beta}, N'_b\}$. Putting the above analysis together, the expected T_{loss} is no more than $\frac{1}{|\mathbb{S}_{prk}|}(\frac{I_t - I_{prk}}{P_0 \times \beta} + \frac{I'_t - I'_{prk}}{P'_0 \times \beta})$. □

Proposition 5.3 enables us to compute the upper bound, denoted by T_{lb}, on the throughput loss in PRK-based scheduling. For convenience, we let $\Delta X = \min\{\frac{I_t - I_{prk}}{P_0 \times \beta}, N_b\} + \min\{\frac{I'_t - I'_{prk}}{P'_0 \times \beta}, N'_b\}$, and thus $T_{lb} = \frac{\Delta X}{|\mathbb{S}_{prk}|}$. Note that ΔX represents an upper bound on $|\mathbb{S}_{prk} \setminus \mathbb{S}_{sinr}|$, that is, the average number of nodes per exclusion region that are silenced in PRK-based scheduling but not in SINR-based scheduling. In the next subsection, we numerically analyze the properties of ΔX and T_{lb}.

5.2. Numerical analysis

Using the same network and environmental settings of Section 4.1.1 and based on Proposition 5.3, we analyze the throughput loss in PRK-based scheduling as compared with SINR-based scheduling. For each of the system configurations we study, more specifically, we first find I_t, I'_t, and the minimum K value of the PRK model for satisfying certain link reliability requirement, then we compute $|\mathbb{S}_{prk}|$, I_{prk}, and I'_{prk} which in turn enable us to compute ΔX and T_{lb} according to Proposition 5.3. *The observations in grid networks and random networks are similar, thus here we only present results for grid networks; detailed results for random networks can be found in our technical report [Zhang et al. 2012].*

For each system configuration, we compute the ΔX and throughput loss in PRK-based scheduling. For different requirements on packet delivery rate (PDR), Figure 9 shows the boxplot of throughput loss in PRK-based scheduling in different system configurations. We see that *the throughput loss is small in general, and it also tends to decrease as the PDR requirement increases*. For instance, the median throughput loss is less than 5% when the required PDR is 50%, and the median throughput loss is less than 1% when the required PDR is 90%. These findings imply that, for mission-critical wireless networking where the PDR requirement is usually high, PRK-based scheduling can enable a performance very close to what is possible with SINR-based scheduling.

The reason why throughput loss is low in the PRK model is because ΔX tends to be small. For instance, Figure 10 shows, for different PDR requirements, ΔX in different system configurations. We see that ΔX is less than 1 in more than 99% of the system configurations we study.

Our findings suggest that PRK-based scheduling can perform very well compared with SINR-based scheduling: PRK-based scheduling enables a network throughput very close to what is possible in SINR-based scheduling while ensuring the same required PDR. The performance of PRK-

based scheduling also improves as the PDR requirement increases, which implies that PRK-based scheduling can perform well in mission critical wireless networks such as those for real-time, reliable sensing and control.

6. MEASUREMENT STUDY OF PRK- AND SINR-BASED SCHEDULING

Our analytical results show that the PRK model serves well as the basis of instantiating the ratio-K model in different network and environmental settings and that PRK-based scheduling achieves a spatial throughput close to what is possible in SINR-based scheduling. To corroborate these results, we experimentally compare the performance of PRK- and SINR-based scheduling using the *NetEye* wireless sensor network testbed [Ju et al. 2012] at Wayne State University and the *MoteLab* testbed [Werner-Allen et al. 2005] at Harvard University, and we also experimentally verify the tradeoff between reliability and throughput in both PRK- and SINR-based scheduling. To reflect the impact of link-layer behavior on network-wide behavior, we also consider end-to-end throughput in this section. The purposes of this measurement evaluation are to verify the analytical insight and to correct the misconceptions about the potential performance of ratio-K-based scheduling, thus our evaluation will be based on the centralized scheduling algorithm Longest-Queue-First (LQF) that has been used to compare different wireless interference models by Maheshwari et al. [Maheshwari et al. 2008]. Distributed protocol design via the PRK model is a part of our future work.

6.1. Methodology

We use both the NetEye and the MoteLab testbeds so that we can evaluate PRK- and SINR-based scheduling in different network and environmental settings. In what follows, we first describe properties of the two testbeds, then we discuss the traffic patterns and the scheduling objectives studies here.

NetEye testbed. NetEye [Ju et al. 2012] is deployed in an indoor office as shown in Figure 11. We use a 10×12 grid of TelosB motes in NetEye, where every two closest neighboring motes are separated by 2 feet. Each of these TelosB motes is equipped with a 3dB signal attenuator and a 2.45GHz monopole antenna. In our measurement study, we set the radio transmission power to be -25dBm (a.k.a. power level 3 in TinyOS) such that multihop networks can be created. In addition to grid networks, the 10×12 grid enables us to experiment with random networks, where a random network is generated out of the 10×12 grid by removing each mote of the grid with certain probability.

Part of the input to PRK- and SINR-based scheduling algorithms (to be discussed in Section 6.2) are radio model, background noise at every node, and strength of signals from any one node to every other node. To collect these information about the 10×12 grid in NetEye, we perform the following experiment: let the 120 motes take turns to be a transmitter one at a time; when a mote is a transmitter, it broadcasts 600 128-byte packets with a transmission power of -25dBm and an inter-packet interval of 100ms (note: each packet transmission takes $\sim$4ms); while a mote is transmitting packets, every other mote keeps sampling its radio RSSI once every 2ms whether or not it can receive packets from the transmitter, and, if a mote can receive packets from the transmitter, it

Figure 11: *NetEye* wireless sensor network testbed

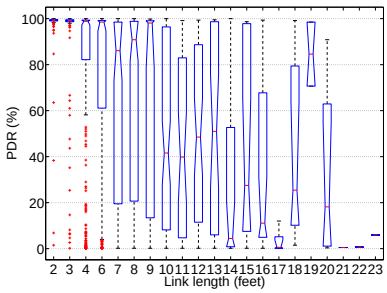

Figure 12: PDR vs. link length in NetEye when transmission power is -25dBm

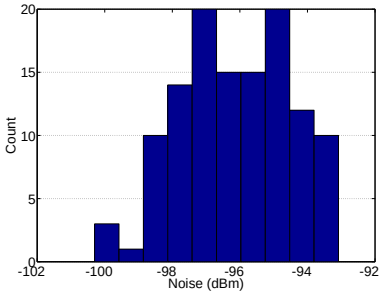

Figure 13: Histogram of background noise power in NetEye

logs the received packets. Using the data collected in this experiment, we can derive the background noise power at each node,[12] the strength of signals from any node to every other node, and the packet delivery rate (PDR) from any node to every other node as well as the associated SINR. These data also enable us to derive the empirical radio model for the TelosB motes in NetEye, and the radio model shows the relation between PDR and SINR. We will use this radio model in our scheduling algorithms for two purposes: 1) to choose the SINR threshold for satisfying certain link reliability, and 2) to compute the expected PDR for a given SINR at a receiver. For the transmission power of -25dBm, Figure 12 shows the boxplot of PDR for links of different length, and Figure 13 shows the histogram of background noise power in NetEye. We see that there is a high degree of variability in PDR for links of equal length and in background noise power. Thus the testbed enables us to do experiments in non-uniform settings.

MoteLab testbed. MoteLab is deployed at three floors of the EECS building of Harvard. Our experiments use all of the 101 operational Tmote Sky motes, with 32, 39, and 30 motes distributed at the first, second, and third floors respectively. We use a transmission power of $-1dBm$ (a.k.a. power level 27) to generate a well-connected multi-hop networks.

Using a method similar to that for NetEye, we have characterized the empirical radio model, background noise at every node, and strength of signals from any node to every other node in MoteLab. Figure 14 shows the histograms of the PDRs of all the wireless links, and Figure 15 shows the histogram of background noise power in MoteLab. We see that there is a high degree of variability in link PDRs and background noise power. Thus the testbed enables us to do experiments in non-uniform settings too.

Traffic patterns. To generate the traffic load for scheduling, we consider convergecast in wireless sensor networks where data packets generated by all the nodes need to be delivered to a base station node.

For NetEye, we consider convergecast in both grid and random networks. For grid network, we let the node at one corner serve as the base station to which the remaining nodes of the 10×12 grid deliver their packets (mostly via multi-hop paths); we generate the random network out of the 10×12 grid by removing a mote in the grid with 30% probability, and then we let a mote closest to a corner of the original grid be the base station (with ties broken randomly). In both the grid and random networks, an approximate routing tree is built by letting each mote choose as its parent the mote having the minimum ETX (i.e., expected transmission count) value to the base station among all the motes within 6 feet distance. Given a routing tree, we generate the traffic load as follows: each node generates a packet with 50% probability, and then the number of packets that need to be delivered across a link is the number of packets generated in the subtree rooted at the transmitter

[12] It is derived from RSSI readings in the absence of packet transmission.

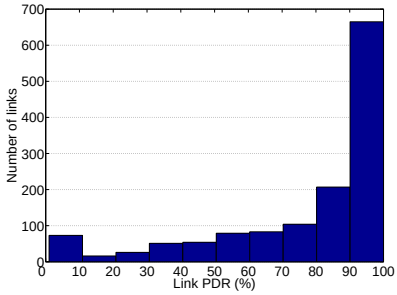

Figure 14: Histogram of link PDRs in MoteLab

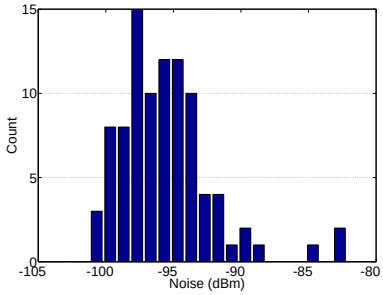

Figure 15: Histogram of background noise power in MoteLab

of the link. Then the traffic load is used as the input to PRK- and SINR-based scheduling. (Note that this traffic load can simulate event detection and may also be repeated to simulate periodic data collection in sensor networks.)

For MoteLab, we let mote #115 at the center of the second floor be the base station to which the remaining 100 motes deliver their packets (mostly via multi-hop paths). Then the routing tree and network traffic are generated in the same manner as in NetEye.

Scheduling objectives. When scheduling the aforementioned traffic load, we consider three different scheduling objectives: 1) *Obj-5*: to guarantee a 5dB minimum SINR at transmitters and receivers (with throughput maximization as a second-order objective), which corresponds to a link PDR of $\sim$88% and $\sim$97% in NetEye and MoteLab respectively; 2) *Obj-8*: to guarantee an 8dB minimum SINR at transmitters and receivers, which corresponds to a link PDR of $\sim$95% and $\sim$98% in NetEye and MoteLab respectively; and 3) *Obj-T*: to maximize network throughput. When comparing PRK- and SINR-based scheduling for different objectives and networks, we consider both link PDR and network throughput.

Overall, we have 12 different experiment configurations, where each configuration specifies a scheduling objective, a topology, and an interference model. A schedule is generated by our scheduling algorithms for each system configuration, where the schedule $S = \{S_1, S_2, \ldots, S_\tau\}$, with S_j being a set of links scheduled in j-th time slot and τ being the schedule length. Experiment with each schedule is repeated 10 times to gain statistical insight. To experiment with a schedule in NetEye, we select a mote not in the 10×12 grid to be the commander that broadcasts the schedule, slot by slot, to the motes involved (as either a transmitter or a receiver) in each slot such that the links in the same lot are synchronized to transmit at the same time; each slot is repeated 30 times before moving onto the next slot so that we can get 30 samples on the transmission status (i.e., success or failure) along each link of the slot to understand the behavior of each slot.

In the next subsection, we describe the scheduling algorithms used in our evaluation.

6.2. Scheduling algorithms

Optimal SINR- and ratio-K-based scheduling are NP-complete in general [Chafekar et al. 2008; Sharma et al. 2006], thus we use the greedy, approximate scheduling framework, denoted by Longest-Queue-First (LQF) [Joo et al. 2008; Le et al. 2010; Blough et al. 2008],[13] that has been

[13]Note that the LQF scheduling framework has been shown to achieve close-to-optimal throughput in many practical scenarios [Joo et al. 2008; Le et al. 2010] and has been a research focus in recent years. Besides LQF, we have also experimented with other scheduling algorithms such as the commonly-used GreedyPhysical [Brar et al. 2006; Wang et al. 2006] and the recently proposed iOrder [Che et al. 2011] algorithm. Similar phenomena have been observed for different algorithms, and here we only present the results based on LQF for conciseness; interested readers can find the results based on GreedyPhysical and iOrder in Appendix D.

used to compare different wireless interference models in literature [Maheshwari et al. 2008]. In addition to interference model, LQF takes as input the link demand vector $f = (f_1, f_2, \ldots, f_L)$ for L number of links, where the demand f_i for the i-th link is the number of packets to be transmitted across the link. The output of LQF is a schedule $S = \{S_1, S_2, \ldots, S_\tau\}$, where S_j is a set of links scheduled in the j-th time slot. LQF works as follows to generate the output schedule:

1. Order and rename links such that $f_1 \geq f_2 \geq \ldots \geq f_L$.
2. Set $i = 1, S = \emptyset, \tau = 0$. (Note: initial schedule is empty.)
3. Schedule link i in the very first available time slot to which link i can be added based on certain scheduling objective (e.g., guaranteeing certain minimum link reliability or maximizing network throughput) and interference model. If no such slot exists, increment τ and schedule link i in the newly created slot. (Note: increasing τ is equivalent to creating a new empty slot at the end of the current schedule.)
4. Repeat step 3 f_i times.
5. Increment i. Go back to step 3 until $i > L$.

For scheduling based on the SINR model, we can use LQF without any modification [Maheshwari et al. 2008; Maheshwari et al. 2009], and we only need to instantiate LQF in the following manner: at step 3, link i can be added to a slot j if 1) the SINR at all the receivers and senders of the slot is above certain threshold γ_0 when the scheduling objective is to guarantee certain minimum link reliability, or 2) if adding link i can increase the expected throughput in slot j when the scheduling objective is to maximize network throughput only. For convenience, we denote this SINR-based scheduling algorithm LQF$_{sinr}$.

For PRK-based scheduling, we need to extend LQF to accommodate the special properties of the PRK model. Given two links l and l', we define the s-distance from l to l', denoted by $sd(l, l')$, as $\min_{n \in \{l.t, l.r\}, n' \in \{l'.t, l'.r\}} sd(n, n')$ where $l.t$ and $l'.t$ are the transmitter of l and l' respectively and $l.r$ and $l'.r$ are the receiver of l and l' respectively. Accordingly, for any three links l, l', and l'', l'' is regarded s-closer to l' than l is if $sd(l'', l') < sd(l, l')$. Then, for every link i' in a slot S_j in PRK-based scheduling, the s-radius of the exclusion region of i' in S_j is less than $\min_{l \in S_j, l \neq i'} sd(l, i')$. When link i cannot be added to any of the existing slots in step 3 of LQF, link i (more precisely, the transmitter and/or the receiver of i) may be within the exclusion region of another link already scheduled. When the scheduling objective is to ensure certain minimum link reliability, link i is within the exclusion region of another link i' in a slot S_j if 1) there is no other link $i'' \in S_j$ that is s-closer to i' than i is, and 2) the SINR at the transmitter or receiver of i' becomes less than certain threshold γ_0 (to violate the link reliability requirement) if we add i to S_j. When the scheduling objective is to maximize network throughput, link i is regarded as within the exclusion region of link i' in S_j if 1) there is no other link $i'' \in S_j$ that is s-closer to i' than i is, and 2) the local throughput of i' decreases if we add i to S_j, where the local throughput of i' is defined as $T_{i'}$ (see Equation 5) divided by the number of nodes in the exclusion region of i'. If i is within the exclusion region of i', we say that the exclusion region of i' covers i.

Let S' be the set of existing slots when link i is being scheduled in step 3 of LQF but cannot be added into any one of S'. Had S' only include one slot S_j ($j = 1, 2, \ldots, |S'|$), then according to the definition of the PRK model, for every link $i' \in S_j$ whose exclusion region covers i, we should remove from S_j every link $i'' \in S_j$, if any, with $sd(i'', i') = sd(i, i')$ so that the exclusion region of i' is well defined in S_j according to the PRK model; this is because, in the PRK model, all the concurrent transmitters of certain s-distance to a transmitter or receiver R, denoted by $\mathcal{S}_0$, are regarded as interferers to R and need to be silenced as long as any node in $\mathcal{S}_0$ has to be silenced for ensuring certain ACK or packet reception reliability at R; we denote all such removed links as $\mathbb{L}(S_j, i)$, and note that $\mathbb{L}(S_j, i)$ may be empty. To make the exclusion region of every link in every slot of S' well defined while minimizing the number of links that have to be removed from the existing slots (for the purpose of high throughput), we need to find the slot $S_{j'}$ such that $|\mathbb{L}(S_{j'}, i)| \leq |\mathbb{L}(S_j, i)|$ for all $j = 1, 2, \ldots, |S'|$; then we regard link i as being silenced by some link $i' \in S_{j'}$,

which entails the generation of a new slot for i. We denote $\mathbb{L}(S_{j'}, i)$ as $\mathbb{L}(i)$; to conform to the PRK model, we need to reschedule every link in $\mathbb{L}(i)$, if non-empty, in step 3 of LQF. Therefore, the PRK-based instantiation of LQF becomes as follows, which is the same as LQF$_{sinr}$ except for the italicized part of step 3:

1. Order and rename links such that $f_1 \geq f_2 \geq \ldots \geq f_L$.
2. Set $i = 1, S = \emptyset, \tau = 0$.
3. Schedule link i in the very first available time slot to which link i can be added based on certain scheduling objective and PRK interference model. If no such slot exists, increment τ and schedule link i in the newly created slot; *additionally, remove* $\mathbb{L}(i)$*, if non-empty, from an existing slot and reschedule them using step 3.*
4. Repeat step 3 f_i times.
5. Increment i. Go back to step 3 until $i > L$.

For convenience, we denote this algorithm as LQF$_{prk}$.

6.3. Experimental results

In what follows, we present the measurement results for NetEye and MoteLab respectively.

NetEye testbed. Using the scheduling algorithms LQF$_{prk}$ and LQF$_{sinr}$, we have measured the performance of PRK- and SINR-based scheduling using the methodology discussed in Section 6.1. Figures 16 and 17 show the PDR and end-to-end throughput of PRK- and SINR-based scheduling in the grid network and the random network respectively, with the error bars representing the 95% confidence intervals (which are very small) of the corresponding metrics. The PDR is defined as the number of successfully delivered packets divided by the number of packets transmitted in a schedule; the end-to-end throughput is defined as the number of successfully delivered packets divided by the schedule length (i.e., number of slots used in a schedule).[14] Note that the throughput is not that high because of the limited concurrency allowed in the testbed which is in turn due to the wide transitional region of wireless communication as can be seen from Figure 12. For instance, Table III shows the probability of having different number of concurrent links in a slot in PRK-based scheduling for the random network and the *Obj-8* objective.

We see that, in agreement with our analytical insight, there is inherent tradeoff between reliability and throughput in both PRK- and SINR-based scheduling. As the scheduling objective moves from

[14] We have also comparatively studied the PDRs of individual links as well as the spatial throughput in PRK- and SINR-based scheduling, and we observe similar phenomena as shown in Figures 16(a) and 17(a). Thus we only present data on end-to-end behavior here.

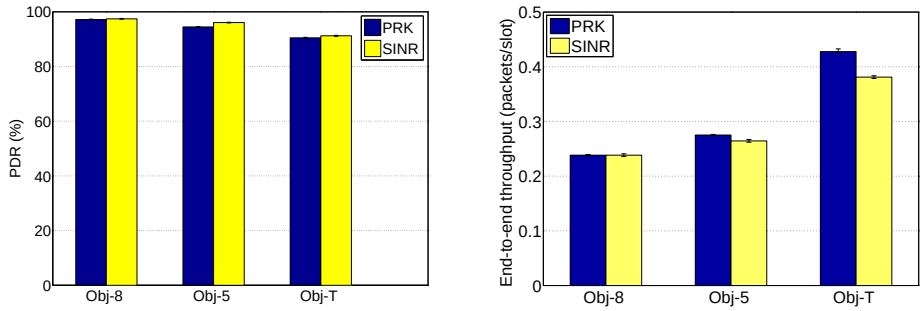

(a) PDR (b) End-to-end throughput

Figure 16: PDR and throughput in the grid network

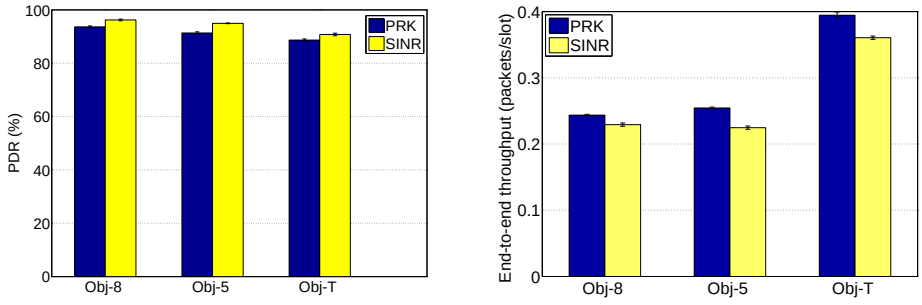

(a) PDR (b) End-to-end throughput

Figure 17: PDR and throughput in the random network

# of Concurrent Links	1	2	3
Probability	0.46	0.51	0.03

Table III: Probability of having different number of concurrent links in a slot: random network, PRK, *Obj-8*

Obj-8 to *Obj-5* and to *Obj-T*, for instance, the throughput in PRK- and SINR-based scheduling keeps increasing, but the PDR keeps decreasing accordingly.

We also see that the performance of PRK-based scheduling is very close to that of SINR-based scheduling, thus the PRK model is able to address the drawbacks of the ratio-K model as observed in [Maheshwari et al. 2008]. The PDRs of PRK- and SINR-based scheduling are above the required link reliability for objectives *Obj-8* and *Obj-5* except for cases that we will discuss in the next paragraph. The PDR in PRK-based scheduling is slightly lower than that in SINR-based scheduling, and, due to reliability-throughput tradeoff, the throughput tends to be slightly higher in PRK-based scheduling. The reason why PRK-based scheduling tends to have slightly lower PDR and higher throughput is because PRK schedules are slightly shorter (e.g., by 3-4 slots less) than SINR schedules, and this is enabled by the fact that silencing/removing links closer-by in the PRK model allows more concurrently transmitting remote links (as discussed in Proposition 5.1). Note that LQF is one of the best known algorithms for SINR-based scheduling [Joo et al. 2008; Le et al. 2010]; the reason why SINR-based scheduling has slightly lower throughput than PRK-based scheduling is because of the reliability-throughput tradeoff in interference-oriented scheduling and not because of the bad performance of LQF itself.

Note that the measured PDRs of the PRK and SINR schedules slightly differ, sometimes higher and sometimes lower, from the PDRs predicted via the radio model and the required SINR threshold when we run the scheduling algorithms LQF$_{prk}$ and LQF$_{sinr}$. This is because 1) wireless link properties (e.g., attenuation) change over time, and the schedule generated based on historical trace data may well behave differently as network condition changes, 2) the radio model itself evolves over time [Sha et al. 2009], and 3) the generated schedule may not be the tightest tessellation of concurrent transmitters, and the SINR at receivers of a schedule may well be greater than the required minimum SINR threshold as shown in Figure 18. Therefore, it is important to adapt to in-situ network and environment conditions in scheduling. It is expected that the locality and high fidelity of the PRK model will enable new approaches to distributed, interference-oriented MAC protocol design, and we will study this issue in our future work.

Together with the above factors, the fact that LQF$_{sinr}$ and LQF$_{prk}$ are approximate algorithms and do not guarantee the optimality of the resulting schedules also explains why PRK schedules

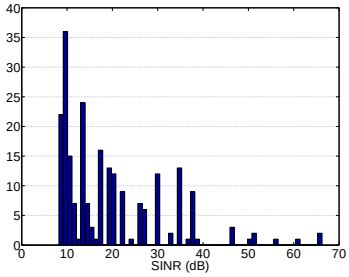

Figure 18: Histogram of receiver-side SINRs in a PRK schedule for the random network and *Obj-8*

have slightly lower PDRs and higher throughput than SINR schedules even though the latter should have higher PDRs based on the analysis of Section 5. For instance, both PRK and SINR schedules ensure the minimum SINR threshold at receivers, but the actual SINRs at the receivers of SINR schedules are higher than those in PRK schedules; thus PDRs are higher in SINR schedules, and the reliability-throughput tradeoff leads to slightly lower throughput in SINR-based scheduling.

MoteLab testbed. Even though the network, traffic, and environmental settings are different for NetEye- and MoteLab-based measurement studies, we observe similar phenomena in MoteLab as those in NetEye. For instance, Figure 19 shows the PDR and throughput for PRK- and SINR-

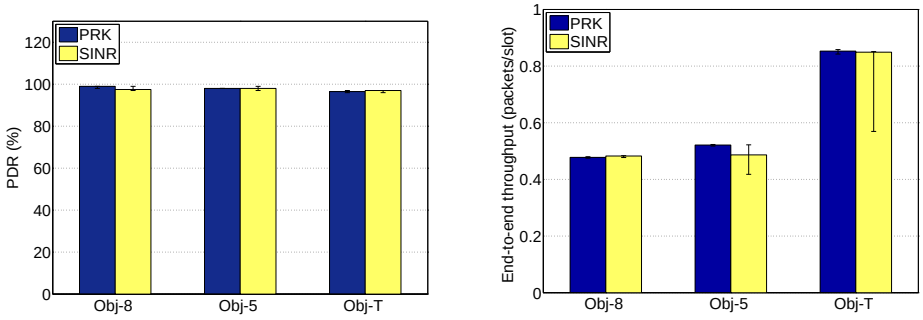

(a) PDR (b) End-to-end throughput

Figure 19: PDR and throughput in MoteLab

based scheduling in MoteLab. The figure shows the tradeoff between link reliability and network throughput in scheduling; it also shows that PRK-based scheduling enables a throughput similar to what is feasible in SINR-based scheduling while ensuring the required link reliability.

7. DISCUSSION

In this section, we examine the ratio-K and the PRK models via simulation with finite TelosB networks. We also analyze the interference modeling issues for UWB networks.

7.1. Simulation with finite networks

Given a set of concurrent transmissions in a finite network, the interference at different receivers may be different depending on their positions in the network. Therefore, the link reliability tends to vary across different links, and the throughput defined by Formula 6 becomes a local metric

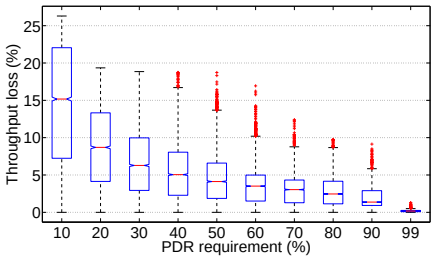

Figure 20: Throughput loss in PRK-based scheduling: finite grid networks

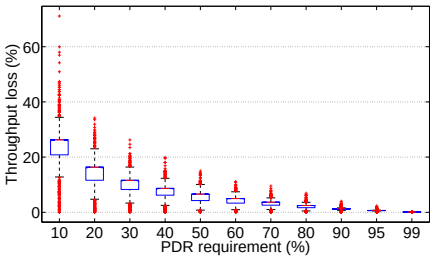

Figure 21: Throughput loss in PRK-based scheduling: UWB grid networks

representing only the local spatial throughput around the neighborhood of a link. Accordingly, the minimum K required to satisfy certain link reliability, denoted by K_{min}, and the optimal K to maximize the local spatial throughput, denoted by K_{opt}, tends to vary across different links of the network. Usually, interference at the center of a network tends to be greater than that at network boundary, thus K_{min} and K_{opt} for links at network center tend to be different from those for links at network boundary. For convenience, we call this phenomenon the *boundary effect*, which does not exist in the uniform, infinite networks studied in Sections 3, 4, and 5. To understand whether the observations in Sections 3, 4, and 5 apply to finite networks, we study the issues of boundary effect, ratio-K instantiation, and the optimality of the PRK model in finite networks using Matlab simulation.

We consider the same system configurations studied in Section 4.1.1 except for the following changes: 1) to understand boundary effect, we add another network parameter N to denote network size (i.e., number of nodes in a network), and the set of Ns we consider are $\{64, 144, 256, 400, 576, 784, 1024, 12961600, 1936, 2304, 2704, 3136, 3600, 4096, 4624, 5184, 5776, 6400, 7056\}$; 2) to reduce simulation time, we only consider the 5 link lengths of $\{1m, 2m, 6m, 10m, 14m\}$ and the 10 node transmission probabilities (i.e., β) of $\{0.1, 0.2, 0.3, 0.4, 0.5, 0.6, 0.7, 0.8, 0.9, 1\}$. The observations in grid and random networks are similar, thus we only present the data for grid networks here.

Our simulation results show that the observations in infinite networks carry over to finite networks despite the potential boundary effect in finite networks. Due to the limitation of space, here we only present Figure 20 which shows the small throughput loss in PRK-based scheduling as compared with SINR-based scheduling, especially when PDR requirement is high.

7.2. Ultra-wideband networks

To understand whether the observations for IEEE 802.15.4 networks carry over to other wireless networks. We analyze the interference modeling issues in IEEE 802.15.4a-based ultra-wideband (UWB) networks. When analyzing UWB networks, we use the same methods as those in Sections 3, 4, and 5, and we consider the same set of system configurations as in Section 4.1.1 except for the following: 1) we replace the CC2420 radio model with the IEEE 802.15.4a DS-UWB radio model used in [Zhang and Brown 2008], 2) we use the typical channel models for UWB networks as specified in [802.15.4a Working Group]. Our analyses show that the observations for TelosB networks apply to UWB networks, even though the specific optimal K for maximizing throughput and the minimum K for satisfying certain link reliability in UWB networks tend to be less than those in TelosB networks due to the higher interference tolerance capability of UWB radios. Due to the limitation of space, here we only present Figure 21 which shows, for grid networks, the small throughput loss in PRK-based scheduling as compared with SINR-based scheduling, especially when PDR requirement is high.

8. RELATED WORK

Maheshwari et al. [Maheshwari et al. 2008] and Moscibroda et al. [Moscibroda et al. 2006] have studied the benefits of SINR-based scheduling as compared with ratio-K-based scheduling. Without studying the impact of different factors and the tradeoff between reliability and throughput in ratio-K-based scheduling, however, these work did not study how to best use the ratio-K model. Focusing on wireless sensing and control networks and based on comprehensive study of the behavior of ratio-K-based scheduling (in particular, the tradeoff between reliability and throughput), we propose the PRK interference model as a basis of adapting K to network and environmental dynamics in ratio-K-based scheduling. We have also studied the optimality of PRK-based scheduling through analysis, simulation, and testbed-based measurement.

Most closely related to our work is Shi et al. [Shi et al. 2009] who, in parallel with our study, examined the effectiveness of the protocol interference model for frequency scheduling (together with routing and power control). Having not focused on distributed protocol design, however, Shi et al. left it as a challenging open problem on how to efficiently choose optimal K in instantiating the ratio-K model, and the optimal K was searched by solving a series of centralized optimization problems in [Shi et al. 2009]. Through detailed study on the sensitivity of and the inherent tradeoff between throughput and reliability in ratio-K-based scheduling, we discover the simple, distributed, link reliability-based approach to instantiating the ratio-K model, and we propose the PRK model which has both the locality of the ratio-K model and the high fidelity of the SINR model. Orthogonal to the focus of Shi et al. [Shi et al. 2009], our work also examines the effectiveness of ratio-K-based scheduling from the perspective of time scheduling and distributed protocol design, studies why PRK/ratio-K-based scheduling can be very close to the performance of SINR-based scheduling, examines the issue in wireless sensing and control networks with a wide range of system configurations (on factors such as traffic load, link length, and wireless signal attenuation), and corroborates the analytical and simulation results with testbed-based measurement.

Other approximate interference models such as hop-based model [Rhee et al. 2006] and range-based model [Wang et al. 2006] have also been used in the literature, but they are either similar or inferior to the ratio-K model [Maheshwari et al. 2008]. Therefore, we did not study those approximate models in this paper. Katz et al. [Katz et al. 2008] studied the feasibility of local interference model, where only nodes in a local neighborhood (with diameter ρ) need to coordinate with one another to ensure minimum SINR at each receiver. But they did not study the impact of various factors on the optimal ρ, nor did they study how to correctly instantiate ρ in dynamic, potentially unpredictable network and environmental settings. Spatial reuse control based on the concept of exclusion region has been studied too [Menon et al. 2006; Ma et al. 2005]. Nonetheless, the issue of the optimal Ks in different scenarios and the comparison between ratio-K- and SINR-based scheduling were not studied in these work. Most of these work have also only focused on exclusion regions around receivers, but not on exclusion regions around both the transmitters and receivers of data transmissions at the same time to ensure reliable delivery of both data and ACK.

Several studies [Gollakota and Katabi 2008; Halperin et al. 2008] recently proposed mechanisms for interference cancellation where a single receiver could simultaneously receive packets from multiple senders. These results challenge the traditional paradigm where a receiver can only receive one packet at a time, and they suggest new ways of interference management. Nonetheless, interference still needs to be controlled due to the constraints of these interference cancellation mechanisms [Li et al. 2010]. For instance, ZigZag decoding [Gollakota and Katabi 2008] works the best when the number of interferers is small (e.g., less than 6). How to schedule transmissions to take advantage of interference cancellation is an interesting problem to study, and there has been some recent effort on this [Li et al. 2010]. But the detailed study of this issue is beyond the scope of this paper.

9. CONCLUDING REMARKS

Through detailed analysis of how different network and environmental factors, such as traffic load and wireless signal attenuation, affect the optimal instantiation of the ratio-K model, we showed

that the performance of ratio-K-based scheduling is highly sensitive to the choice of K and that it is important to take this into account in both protocol design and performance evaluation. We then comparatively studied the performance of PRK- and SINR-based scheduling and showed that, if correctly instantiated via the PRK model, ratio-K-based scheduling can achieve a close-to-optimal performance. Our findings on PRK-based scheduling and the inherent tradeoff between reliability and throughput suggest that the ratio-K model can be effectively instantiated through link-reliability-based adaptation of K, which is amenable to distributed, local implementation too. These findings showed the feasibility of integrating the high fidelity of the SINR model with the locality of the ratio-K model, and suggested new approaches to MAC protocol design in dynamic, unpredictable network and environmental settings. Thus these findings opened up new opportunities and perspectives on interference-oriented protocol design and analysis in wireless sensing and control networks, and we will explore these opportunities in our future work.

ACKNOWLEDGMENTS

We thank the editor and the anonymous reviewers whose insightful comments have improved the quality of the paper.

APPENDIX

A. ANALYSIS OF THE INTERFERENCE IN RATIO-K BASED SCHEDULING IN GRID NETWORKS

In this appendix, we analyze, for the tightest tessellation of concurrent transmissions in grid networks, the receiver-side interference when different ratio-K models are used. The key to this analysis is to identify the spatial distribution of concurrent transmitters (i.e., interferers), based on which the interference introduced by each interferer can be derived from the distance between the interferer and the receiver. Accordingly, we use a coordinate system where the receiver R is located at the origin and its transmitter is located at location (0,1) (i.e., we treat the link length l from R to its transmitter as the unit of distance). So the distance between R and an interferer n_i at location (x, y) is $\sqrt{x^2 + y^2}$. Then, our main task is to identify the coordinates of all the interferers when different ratio-K models are used for the scheduling in grid networks. In what follows, we analyze the coordinates of interferers in scheduling based on different ratio-K models.

When $K = \sqrt{2}$, Figure 22 shows the spatial distribution of concurrent transmissions. Given a link L, we can find four nodes on the boundary of the exclusion region of link L such that each is involved in a concurrent transmission (either as a sender or as a receiver). By symmetry, we can expand this spatial distribution of concurrent transmissions to the rest of the network, and thus the coordinates of interferers are

$$\begin{cases} x = 2n + Q \\ y = 4m + 1 + 2Q \end{cases}$$

where $m, n \in \mathbb{Z}$, $Q \in \{0, 1\}$ and $m^2+n^2+Q \neq 0$. So the receiver-side interference when $K = \sqrt{2}$ is as follows:

$$I = P_t \times \beta \times \ell^{-\alpha} \times \left(\sum_{\substack{m=-\infty \\ m^2+n^2 \neq 0}}^{\infty} \sum_{n=-\infty}^{\infty} \frac{1}{[(2n)^2+(4m+1)^2]^{\alpha/2}} + \sum_{m=-\infty}^{\infty} \sum_{n=-\infty}^{\infty} \frac{1}{[(2n+1)^2+(4m+3)^2]^{\alpha/2}} \right)$$

For other Ks, we can derive interferers' coordinates in a similar fashion. For conciseness, we ignore the detailed derivation here and only give the results as follows.

When $K = \sqrt{5}$, the spatial distribution of concurrent transmissions is shown in Figure 23, and the coordinates of interferers are

$$\begin{cases} x = 4n + 2Q \\ y = 4m + 1 + 2Q \end{cases}$$

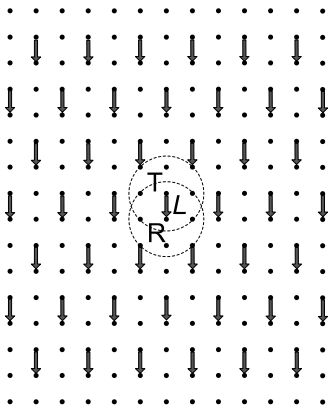

Figure 22: Concurrent transmissions when $K = \sqrt{2}$

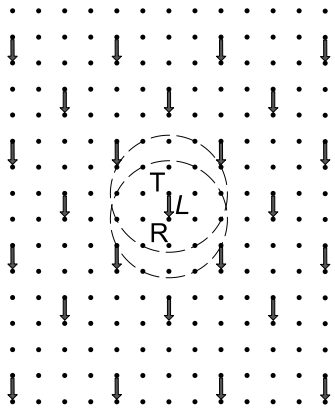

Figure 23: Concurrent transmissions when $K = \sqrt{5}$

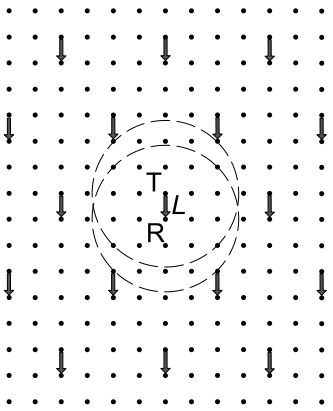

Figure 24: Concurrent transmissions when $K = \sqrt{8}$

where $m, n \in \mathbb{Z}$, $Q \in \{0, 1\}$ and $m^2 + n^2 + Q \neq 0$. So the receiver-side interference is

$$I = P_t \times \beta \times \ell^{-\alpha} \times \left(\sum_{\substack{m=-\infty \\ m^2+n^2 \neq 0}}^{\infty} \sum_{n=-\infty}^{\infty} \frac{1}{[(4n)^2+(4m+1)^2]^{\alpha/2}} + \sum_{m=-\infty}^{\infty} \sum_{n=-\infty}^{\infty} \frac{1}{[(4n+2)^2+(4m+3)^2]^{\alpha/2}} \right)$$

When $K = \sqrt{8}$, the spatial distribution of concurrent transmissions is shown in Figure 24, and the coordinates of interferers are

$$\begin{cases} x = 4n + 2Q \\ y = 6m + 1 + 3Q \end{cases}$$

where $m, n \in \mathbb{Z}$, $Q \in \{0, 1\}$ and $m^2 + n^2 + Q \neq 0$. So the receiver-side interference is

$$I = P_t \times \beta \times \ell^{-\alpha} \times \left(\sum_{\substack{m=-\infty \\ m^2+n^2 \neq 0}}^{\infty} \sum_{n=-\infty}^{\infty} \frac{1}{[(4n)^2+(6m+1)^2]^{\alpha/2}} + \sum_{m=-\infty}^{\infty} \sum_{n=-\infty}^{\infty} \frac{1}{[(4n+2)^2+(6m+4)^2]^{\alpha/2}} \right)$$

When $K = 3$, the spatial distribution of concurrent transmissions is shown in Figure 25, and the coordinates of interferers are

$$\begin{cases} x = 3n \\ y = 4m + 1 \end{cases}$$

where $m, n \in \mathbb{Z}$ and $m^2 + n^2 \neq 0$. So the receiver-side interference is

$$I = P_t \times \beta \times \ell^{-\alpha} \times \left(\sum_{\substack{m=-\infty \\ m^2+n^2 \neq 0}}^{\infty} \sum_{n=-\infty}^{\infty} \frac{1}{[(3n)^2+(4m+1)^2]^{\alpha/2}} \right)$$

When $K = \sqrt{10}$, the spatial distribution of concurrent transmissions is shown in Figure 26 and interferers are divided into 7 groups, denoted as $G_1, G_2, \ldots, G_7$, and we let $I = \sum_{i=1}^{7} I_i$, where I_i is the interference from nodes of group G_i. The coordinates of nodes in G_1 are

$$\begin{cases} x = 7n \\ y = 14m + 1 \end{cases}$$

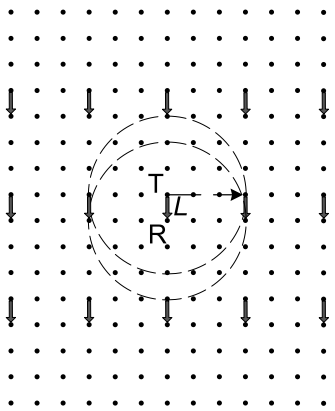

Figure 25: Concurrent transmissions when $K = 3$

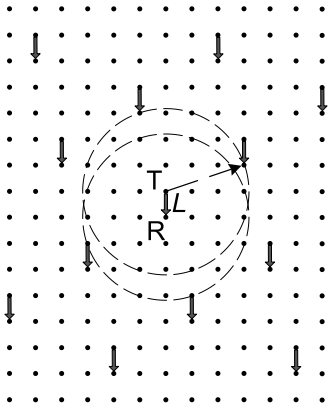

Figure 26: Concurrent transmissions when $K = \sqrt{10}$

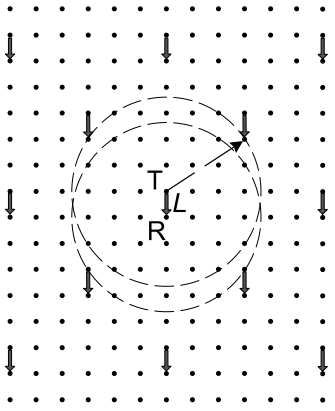

Figure 27: Concurrent transmissions when $K = \sqrt{13}$

where $m, n \in \mathbb{Z}$ and $m^2 + n^2 \neq 0$. And I_1 is given by

$$I_1 = P_t \times \beta \times \ell^{-\alpha} \times \sum_{\substack{m=-\infty \\ m^2+n^2 \neq 0}}^{\infty} \sum_{n=-\infty}^{\infty} \frac{1}{[(7n)^2+(14m+1)^2]^{\alpha/2}}$$

The coordinates of nodes in G_2 are

$$\begin{cases} x = 7n + 4 \\ y = 14m - 1 \end{cases}$$

where $m, n \in \mathbb{Z}$ and $m^2 + n^2 \neq 0$. And I_2 is given by

$$I_2 = P_t \times \beta \times \ell^{-\alpha} \times \sum_{m=-\infty}^{\infty} \sum_{n=-\infty}^{\infty} \frac{1}{[(7n+4)^2+(14m-1)^2]^{\alpha/2}}$$

The coordinates of nodes in G_3 are

$$\begin{cases} x = 7n + 1 \\ y = 14m - 3 \end{cases}$$

where $m, n \in \mathbb{Z}$ and $m^2 + n^2 \neq 0$. And I_3 is given by

$$I_3 = P_t \times \beta \times \ell^{-\alpha} \times \sum_{m=-\infty}^{\infty} \sum_{n=-\infty}^{\infty} \frac{1}{[(7n+1)^2+(14m-3)^2]^{\alpha/2}}$$

The coordinates of nodes in G_4 are

$$\begin{cases} x = 7n + 5 \\ y = 14m - 5 \end{cases}$$

where $m, n \in \mathbb{Z}$ and $m^2 + n^2 \neq 0$. And I_4 is given by

$$I_4 = P_t \times \beta \times \ell^{-\alpha} \times \sum_{m=-\infty}^{\infty} \sum_{n=-\infty}^{\infty} \frac{1}{[(7n+5)^2+(14m-5)^2]^{\alpha/2}}$$

The coordinates of nodes in G_5 are

$$\begin{cases} x = 7n + 2 \\ y = 14m - 7 \end{cases}$$

where $m, n \in \mathbb{Z}$ and $m^2 + n^2 \neq 0$. And I_5 is given by

$$I_5 = P_t \times \beta \times \ell^{-\alpha} \times \sum_{m=-\infty}^{\infty} \sum_{n=-\infty}^{\infty} \frac{1}{[(7n+2)^2+(14m-7)^2]^{\alpha/2}}$$

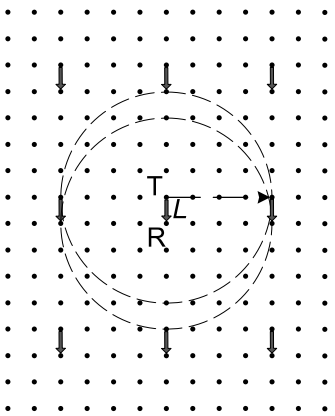

Figure 28: Concurrent transmissions when $K = 4$

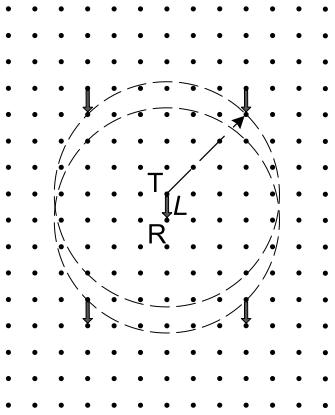

Figure 29: Concurrent transmissions when $K = \sqrt{18}$

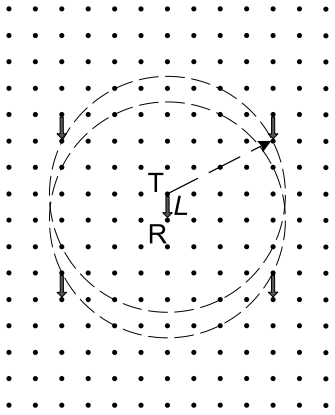

Figure 30: Concurrent transmissions when $K = \sqrt{20}$

The coordinates of nodes in G_6 are

$$\begin{cases} x = 7n + 6 \\ y = 14m - 9 \end{cases}$$

where $m, n \in \mathbb{Z}$ and $m^2 + n^2 \neq 0$. And I_6 is given by

$$I_6 = P_t \times \beta \times \ell^{-\alpha} \times \sum_{m=-\infty}^{\infty} \sum_{n=-\infty}^{\infty} \frac{1}{[(7n+6)^2+(14m-9)^2]^{\alpha/2}}$$

The coordinates of nodes in G_7 are

$$\begin{cases} x = 7n + 3 \\ y = 14m - 11 \end{cases}$$

where $m, n \in \mathbb{Z}$ and $m^2 + n^2 \neq 0$. And I_7 is given by

$$I_7 = P_t \times \beta \times \ell^{-\alpha} \times \sum_{m=-\infty}^{\infty} \sum_{n=-\infty}^{\infty} \frac{1}{[(7n+3)^2+(14m-11)^2]^{\alpha/2}}$$

When $K = \sqrt{13}$, the spatial distribution of concurrent transmissions is shown in Figure 27, and the coordinates of interferers are

$$\begin{cases} x = 4n + 2Q \\ y = 8m + 4Q + 1 \end{cases}$$

where $m, n \in \mathbb{Z}$, $Q \in \{0, 1\}$ and $m^2 + n^2 + Q \neq 0$. So the receiver-side interference is

$$I = P_t \times \beta \times \ell^{-\alpha} \times \left(\sum_{\substack{m=-\infty \\ m^2+n^2 \neq 0}}^{\infty} \sum_{n=\infty}^{\infty} \frac{1}{[(4n)^2+(8m+1)^2]^{\alpha/2}} + \sum_{m=-\infty}^{\infty} \sum_{n=-\infty}^{\infty} \frac{1}{[(4n+2)^2+(8m+5)^2]^{\alpha/2}} \right)$$

When $K = 4$, the spatial distribution of concurrent transmissions is shown in Figure 28, and the coordinates of interferers are

$$\begin{cases} x = 6n \\ y = 5m + 1 \end{cases}$$

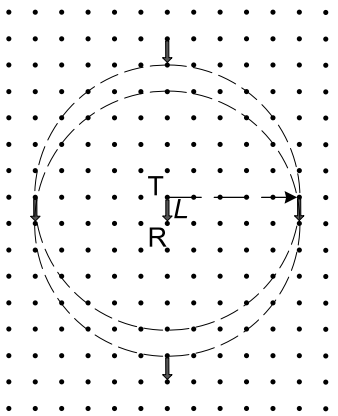

Figure 31: Concurrent transmissions when $K = 5$

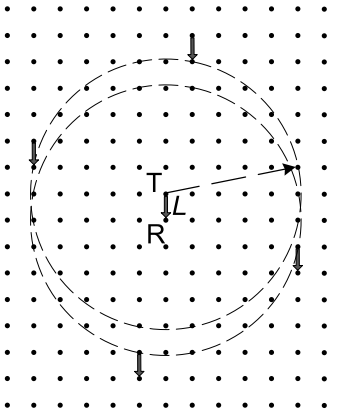

Figure 32: Concurrent transmissions when $K = \sqrt{26}$

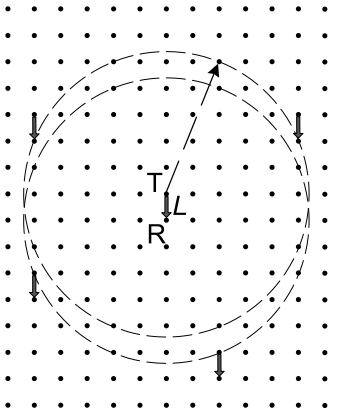

Figure 33: Concurrent transmissions when $K = \sqrt{29}$

where $m, n \in \mathbb{Z}$ and $m^2 + n^2 \neq 0$. So the receiver-side interference is

$$I = P_t \times \beta \times \ell^{-\alpha} \times \left(\sum_{\substack{m=-\infty \\ m^2+n^2 \neq 0}}^{\infty} \sum_{n=-\infty}^{\infty} \frac{1}{[(6n)^2+(7m+1)^2]^{\alpha/2}} \right)$$

When $K = \sqrt{18}$, the spatial distribution of concurrent transmissions is shown in Figure 29, and the coordinates of interferers are

$$\begin{cases} x = 6n + 3Q \\ y = 7m + 3Q + 1 \end{cases}$$

where $m, n \in \mathbb{Z}$, $Q \in \{0, 1\}$ and $m^2 + n^2 + Q \neq 0$. So the receiver-side interference is

$$I = P_t \times \beta \times \ell^{-\alpha} \times \left(\sum_{\substack{m=-\infty \\ m^2+n^2 \neq 0}}^{\infty} \sum_{n=-\infty}^{\infty} \frac{1}{[(6n)^2+(7m+1)^2]^{\alpha/2}} + \sum_{m=-\infty}^{\infty} \sum_{n=-\infty}^{\infty} \frac{1}{[(6n+3)^2+(7m+4)^2]^{\alpha/2}} \right)$$

When $K = \sqrt{20}$, the spatial distribution of concurrent transmissions is shown in Figure 30, and the coordinates of interferers are

$$\begin{cases} x = 8n + 4Q \\ y = 6m + 3Q + 1 \end{cases}$$

where $m, n \in \mathbb{Z}$, $Q \in \{0, 1\}$ and $m^2 + n^2 + Q \neq 0$. So the receiver-side interference is

$$I = P_t \times \beta \times \ell^{-\alpha} \times \left(\sum_{\substack{m=-\infty \\ m^2+n^2 \neq 0}}^{\infty} \sum_{n=-\infty}^{\infty} \frac{1}{[(8n)^2+(6m+1)^2]^{\alpha/2}} + \sum_{m=-\infty}^{\infty} \sum_{n=-\infty}^{\infty} \frac{1}{[(8n+4)^2+(6m+4)^2]^{\alpha/2}} \right)$$

When $K = 5$, the spatial distribution of concurrent transmissions is shown in Figure 31, and the coordinates of interferers are

$$\begin{cases} x = 5n \\ y = 6m + 1 \end{cases}$$

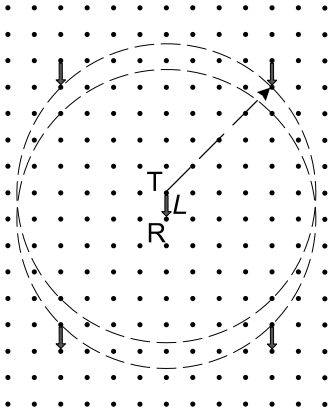

Figure 34: Concurrent transmissions when $K = \sqrt{32}$

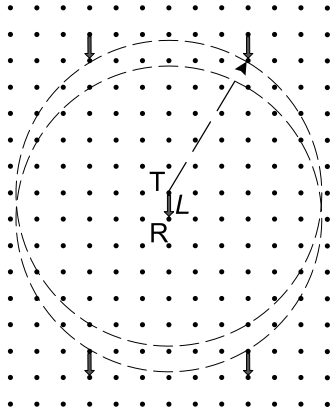

Figure 35: Concurrent transmissions when $K = \sqrt{34}$

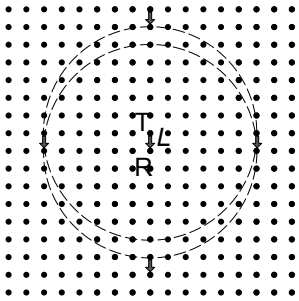

Figure 36: Concurrent transmissions when $K = 6$

where $m, n \in \mathbb{Z}$ and $m^2 + n^2 \neq 0$. So the receiver-side interference is

$$I = P_t \times \beta \times \ell^{-\alpha} \times \left(\sum_{\substack{m=-\infty \\ m^2+n^2 \neq 0}}^{\infty} \sum_{n=-\infty}^{\infty} \frac{1}{[(5n)^2+(6m+1)^2]^{\alpha/2}} \right)$$

When $K = \sqrt{26}$, the spatial distribution of concurrent transmissions is shown in Figure 32, and the coordinates of interferers are

$$\begin{cases} x = 5n + m \\ y = -2n + 6m + 1 \end{cases}$$

where $m, n \in \mathbb{Z}$ and $m^2 + n^2 \neq 0$. So the receiver-side interference is

$$I = P_t \times \beta \times \ell^{-\alpha} \times \left(\sum_{\substack{m=-\infty \\ m^2+n^2 \neq 0}}^{\infty} \sum_{n=-\infty}^{\infty} \frac{1}{[(5n+m)^2+(-2n+6m+1)^2]^{\alpha/2}} \right)$$

When $K = \sqrt{29}$, the spatial distribution of concurrent transmissions is shown in Figure 33, and the coordinates of interferers are

$$\begin{cases} x = 5n + 2m \\ y = 3n - 6m + 1 \end{cases}$$

where $m, n \in \mathbb{Z}$ and $m^2 + n^2 \neq 0$. So the receiver-side interference is

$$I = P_t \times \beta \times \ell^{-\alpha} \times \left(\sum_{\substack{m=-\infty \\ m^2+n^2 \neq 0}}^{\infty} \sum_{n=-\infty}^{\infty} \frac{1}{[(5n+2m)^2+(3n-6m+1)^2]^{\alpha/2}} \right)$$

When $K = \sqrt{32}$, the spatial distribution of concurrent transmissions is shown in Figure 34, and the coordinates of interferers are

$$\begin{cases} x = 8n + 4Q \\ y = 10m + 5Q + 1 \end{cases}$$

where $m, n \in \mathbb{Z}$, $Q \in \{0, 1\}$ and $m^2 + n^2 + Q \neq 0$. So the receiver-side interference is

$$I = P_t \times \beta \times \ell^{-\alpha} \times \left(\sum_{\substack{m=-\infty \\ m^2+n^2 \neq 0}}^{\infty} \sum_{n=-\infty}^{\infty} \frac{1}{[(8n)^2+(10m+1)^2]^{\alpha/2}} + \sum_{m=-\infty}^{\infty} \sum_{n=-\infty}^{\infty} \frac{1}{[(8n+4)^2+(10m+6)^2]^{\alpha/2}} \right)$$

When $K = \sqrt{34}$, the spatial distribution of concurrent transmissions is shown in Figure 35, and the coordinates of interferers are

$$\begin{cases} x = 6n + 3Q \\ y = 12m + 5Q + 1 \end{cases}$$

where $m, n \in \mathbb{Z}$, $Q \in \{0, 1\}$ and $m^2 + n^2 + Q \neq 0$. So the receiver-side interference is

$$I = P_t \times \beta \times \ell^{-\alpha} \times \left(\sum_{\substack{m=-\infty \\ m^2+n^2 \neq 0}}^{\infty} \sum_{n=-\infty}^{\infty} \frac{1}{[(6n)^2+(12m+1)^2]^{\alpha/2}} + \sum_{m=-\infty}^{\infty} \sum_{n=-\infty}^{\infty} \frac{1}{[(6n+3)^2+(12m+6)^2]^{\alpha/2}} \right)$$

When $K = 6$, the spatial distribution of concurrent transmissions is shown in Figure 36, and the coordinates of interferers are

$$\begin{cases} x = 6n \\ y = 7m + 1 \end{cases}$$

where $m, n \in \mathbb{Z}$ and $m^2 + n^2 \neq 0$. So the receiver-side interference is

$$I = P_t \times \beta \times \ell^{-\alpha} \times \left(\sum_{\substack{m=-\infty \\ m^2+n^2 \neq 0}}^{\infty} \sum_{n=-\infty}^{\infty} \frac{1}{[(6n)^2+(7m+1)^2]^{\alpha/2}} \right)$$

B. PROOF OF MAXIMUM-SPATIAL-REUSE TRAFFIC PATTERN IN GRID NETWORKS

In what follows, we prove the fact, used in Section 3, that the uniform traffic pattern where all the transmissions follow the same direction along the grid-line enables the maximum degree of spatial reuse in grid networks.

For convenience, we regard the schedules generated for the traffic pattern where all the transmissions follow the same direction along the grid-line as the *same-direction schedules*, and we regard the schedules generated for the traffic pattern where transmissions follow different directions and different grid-lines as *different-direction schedules*. To achieve maximal spatial reuse, we need to minimize the average area where nodes are silenced due to transmissions along a link. Given a ratio-K model, we find the minimum area-per-link in optimal same-direction schedules and different-direction schedules, and we denote them by $A_{min}(k)$ and $A'_{min}(k)$ respectively. We will show that $A_{min}(k) < A'_{min}(k)$ for all the cases we study.

Given an infinite grid network, we pick one node as the origin to set up the coordinate system. So the coordinate of any node in grid networks, say (x, y), is such that $x, y \in \mathbb{Z}$. As discussed in Section 3, here we only consider cases where link length ℓ is a multiple of grid hop length. For simplicity of presentation in the following discussion, we also set the unit of variables as multiples of ℓ.

Suppose that the coordinates of an end-node of a link and one of its closest interferers are (x, y), (x', y') respectively. In grid networks, the following holds:

$$\begin{cases} |x - x'| = a \\ |y - y'| = b \\ \sqrt{a^2 + b^2} = K \end{cases}$$

where $a, b \in \mathbb{Z}^+$ and K is the parameter of the ratio-K model. The values of a and b in different ratio-K models are shown in Table IV.

Table IV: a and b in ratio-K model

K	(a, b)	K	(a, b)
$\sqrt{2}$	(1, 1)	2	(0, 2)
$\sqrt{5}$	(1, 2)	$\sqrt{8}$	(2, 2)
3	(0, 3)	$\sqrt{10}$	(1, 3)
$\sqrt{13}$	(2, 3)	4	(0, 4)
$\sqrt{18}$	(3, 3)	$\sqrt{20}$	(2, 4)
5	(0, 5)/(3,4)	$\sqrt{26}$	(1, 5)
$\sqrt{29}$	(2, 5)	$\sqrt{32}$	(4, 4)
$\sqrt{34}$	(3, 5)	$\sqrt{6}$	(0, 6)

For same-direction transmissions, there are four possible patterns of tightest spatial reuse, as shown in Figures 37, 38, 39, and 40. Denote these patterns of patter I, II, III, and IV respectively. The average area-per-link for each spatial reuse pattern is shown in Equations 18, 19, 20, and 21 below:

$$A_I(a, b) = (a + 1)(a + b) + b(b - a), \text{if } a > 0, \tag{18}$$

$$A_{II}(a, b) = 2b \times (a + 1), \text{if } 2b > \sqrt{a^2 + b^2}, 2a + 1 > \sqrt{a^2 + b^2} \tag{19}$$

$$A_{III}(a, b) = 2a \times (b + 1), \text{if } 2a > \sqrt{a^2 + b^2}, 2b + 1 > \sqrt{a^2 + b^2} \tag{20}$$

$$A_{IV}(a, b) = b \times (b + 1), \text{if } a = 0 \tag{21}$$

To achieve the highest spatial reuse for same-direction transmissions, we define a set of candidate schedule types $Sch_{a,b} = \{i | (a, b)$ satisfies the requirement of schedule pattern $i, i \in I, II, III, IV\}$. So the average area-per-link is $A_{min} = \min\{A_i, i \in Sch_{a,b}\}$.

For different-direction transmissions, there are also four types of tightest schedules, namely V, VI, VII, and $VIII$ as shown in Figures 41, 42, 43, and 44 respectively. The average area-per-link for each spatial reuse pattern is shown in Equations 22, 23, 24, and 25 as follows.

$$A_V(a, b) = \frac{(a + b + 1)^2 + (b - a)^2}{2}, \text{if } a > 0, \tag{22}$$

$$A_{VI}(a, b) = \frac{(2a + 1)(2b + 1)}{2}, \text{if } 2a \geq \sqrt{a^2 + b^2}, 2b \geq \sqrt{a^2 + b^2} \tag{23}$$

$$A_{VII}(a, b) = \frac{b(3b + a + 2)}{2}, \text{if } a > 0, b = a + 1 \tag{24}$$

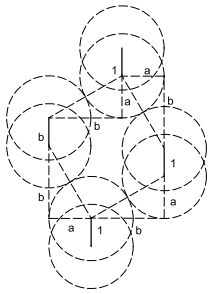

Figure 37: Type I schedule

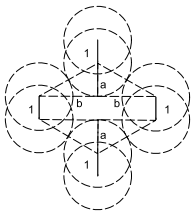

Figure 38: Type II schedule

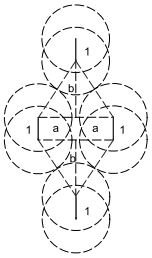

Figure 39: Type III schedule

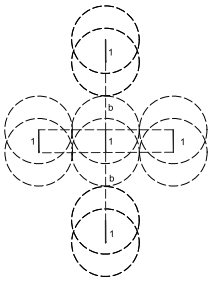

Figure 40: Type IV schedule

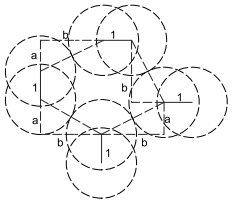

Figure 41: Type V schedule

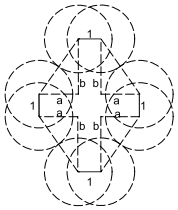

Figure 42: Type VI schedule

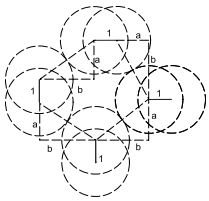

Figure 43: Type VII schedule

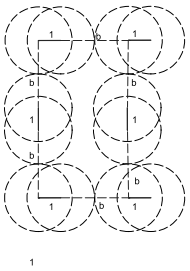

Figure 44: Type $VIII$ schedule

$$A_{VIII}(a,b) = (2b+1)(b+1), \text{if } a = 0 \tag{25}$$

Similar to the case of same-direction transmissions, we define $Sch'_{a,b} = \{i|(a,b)$ satisfies the requirement of schedule pattern $i, i \in V, VI, VII, VIII\}$. So the average area-per-link is $A'_{min} = \min\{A_j, j \in Sch'_{a,b}\}$.

We compute A_{min} and A'_{min} for different ratio-K instantiations, and Table V shows the results. We see that same-direction schedules always have smaller area-per-link than the corresponding different-direction schedules do. This implies that same-direction traffic patterns enable maximum degree of spatial reuse.

C. ANALYSIS OF ONE-HOP DATA DELIVERY DELAY

Here we analyze the single-hop transmission delays when we need to ensure a link layer data delivery reliability of p_0.

To ensure a link layer frame delivery reliability of p_0 when the delivery rate of each transmission is p, a frame may have to be retransmitted. The maximum number of transmissions, denoted by x_0,

Table V: A_{min} and A'_{min} in ratio-K based scheduling

K	$A_{min}(k)$	$A'_{min}(k)$
$\sqrt{2}$	4	4.5
2	6	7.5
$\sqrt{5}$	8	8.5
$\sqrt{8}$	12	12.5
3	12	14
$\sqrt{10}$	12	14.5
$\sqrt{13}$	16	17.5
4	20	22.5
$\sqrt{18}$	24	24.5
$\sqrt{20}$	24	26.5
5	30	33
$\sqrt{26}$	32	32.5
$\sqrt{29}$	36	36.5
$\sqrt{32}$	40	40.5
$\sqrt{34}$	36	38.5
6	42	45.5

can be computed as follows:

$$x_0 = \arg\min_{x \geq 1} \ (1-p)^x \leq 1 - p_0 < (1-p)^{x-1} \tag{26}$$

$$= \begin{cases} 1 & \text{if } p = 1 \\ \lceil \frac{ln(1-p_0)}{ln(1-p)} \rceil & \text{if } 0 < p < 1 \end{cases}. \tag{27}$$

Then, when a frame is to be delivered by the link layer, the frame will be transmitted/retransmitted until it is successfully received by the receiver or the frame has been transmitted for x_0 number of times.

In what follows, we analyze the expected transmission delay when link scheduling is based on TDMA and CSMA respectively.

TDMA Delay. When TDMA scheme is applied, a node will compete with N_{ex} number of nodes in its exclusion region. We assume that the TDMA scheme is fair to all the nodes within the exclusion region. We also assume that each node will only transmit one packet each time it gains the channel and each packet transmission takes one slot time. Then a transmitter has to wait $\frac{N_{ex}}{2}$ slots for the first transmission attempt on average, and $N_{ex}-1$ for every re-transmission attempt after that. Thus, the expectation of a single packet transmission delay, denoted as $T_{d,tdma}$, is

$$\begin{aligned} E[T_{d,tdma}] =& E[t_1] \cdot p + E[t_2] \cdot p(1-p) + ... + E[t_{x_0-1}] \cdot p(1-p)^{x_0-1} + E[t_{x_0}] \cdot (1-p)^{x_0-1} \\ =& \frac{N}{2} + (N-1) \left\{ \frac{1-p}{p} + \left[2x_0 - 1 - \frac{1}{p} \right] \cdot (1-p)^{x_0-1} \right\}, \end{aligned}$$

where $E[t_k] = \frac{N_{ex}}{2} + (k-1)(N_{ex}-1), 1 \leq k \leq x_0$.

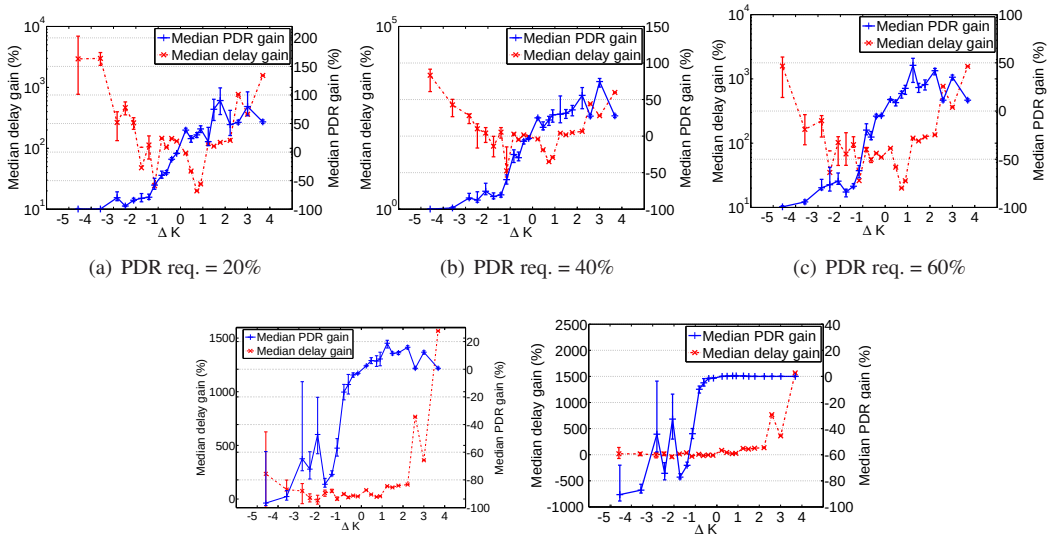

(a) PDR req. = 20% (b) PDR req. = 40% (c) PDR req. = 60%

(d) PDR req. = 80% (e) PDR req. = 99%

Figure 45: Δk vs. performance gain: TDMA, grid networks

Note that the unit of time is a time slot.

CSMA delay. According to [Yedavalli and Krishnamachar 2008], the expected delay between any two transmission can be computed as

$$E[T_n] = \frac{L - (L-1)(1-p_c)^n}{np_c(1-p_c)^{n-1}}\delta,$$

where n is the number of nodes in the exclusion region, L is the length of packet in the number of time slots ($L = 13$ in our study), δ is the duration of a time slot which is 320 microseconds, and p_c is the channel access probability which is approximately $\frac{1}{16.5} = 0.606$ [Yedavalli and Krishnamachar 2008]. Note that $E[T]$ includes the idle time, collision time, and the packet transmission time.

So the expected delay D_{csma} when the link quality is p can be computed as

$$\begin{aligned} E[D_{csma}] =& E[T_n] \cdot p + 2E[T_n] \cdot p(1-p) + ... \\ &+ x_0 \cdot E[T_n] \cdot p(1-p)^{x_0-1} + x_0 \cdot E[T_n] \cdot (1-p)^{x_0} \\ =& E[T_n] \cdot \big(\frac{1+(1-p)^{x_0}}{p} + 2x_0(1-p).^{x_0-1}\big). \end{aligned}$$

Simulation Result. Figures 45, 46, 47, and 48 show the median delay change and its 95% confidence interval in grid and Poisson networks and when the channel access is through TDMA or CSMA. We see that the transmission delay varies significantly when K varies by ΔK from the minimum K' that ensures a certain link reliability. For Poisson networks with TDMA channel access control (see Figure 46(d)), for instance, the median delay gain can be 167% when $\Delta K = -1$. We also observe that choosing the minimum K' that ensures the required link reliability also helps reduce data delivery delay. As K increases from K', the delay increases because the number of nodes in a link's exclusion region increases, which introduces larger contention delay in channel access. As K decreases from K', the contention delay decreases, but the overall delay still increases because retransmissions are required to ensure the same link-layer data delivery reliability as what is enabled by K' without retransmission.

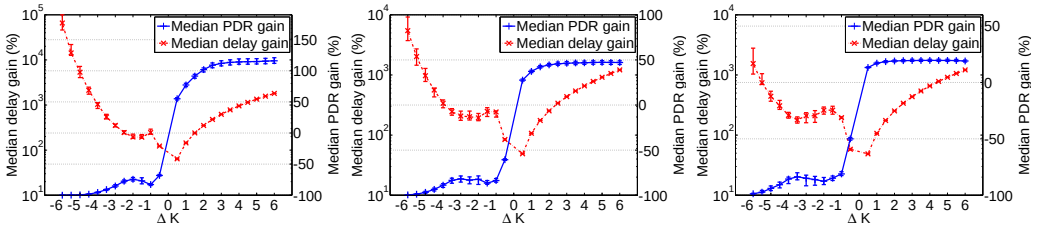

(a) PDR req. = 20% (b) PDR req. = 40% (c) PDR req. = 60%

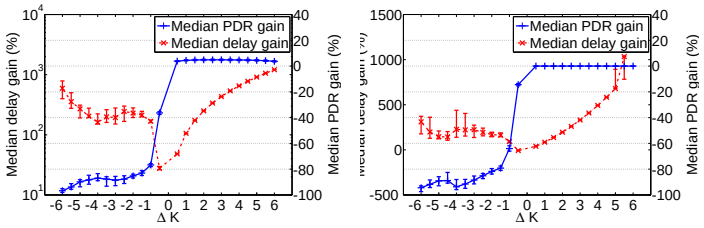

(d) PDR req. = 80% (e) PDR req. = 99%

Figure 46: Δk vs. performance gain: TDMA, Poisson networks

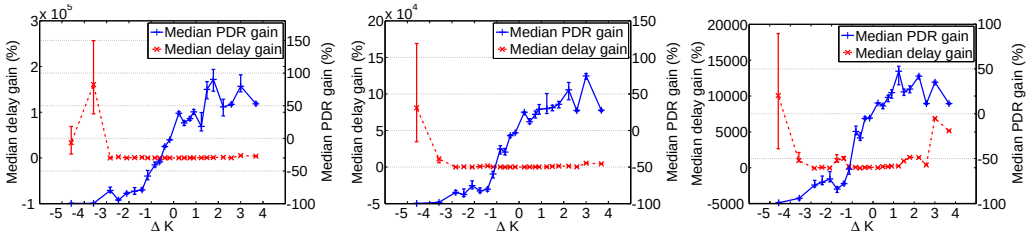

(a) PDR req. = 20% (b) PDR req. = 40% (c) PDR req. = 60%

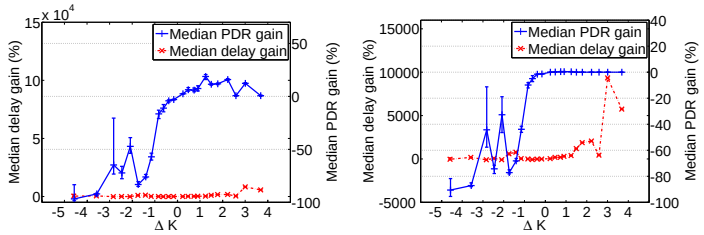

(d) PDR req. = 80% (e) PDR req. = 99%

Figure 47: Δk vs. performance gain: CSMA, grid networks

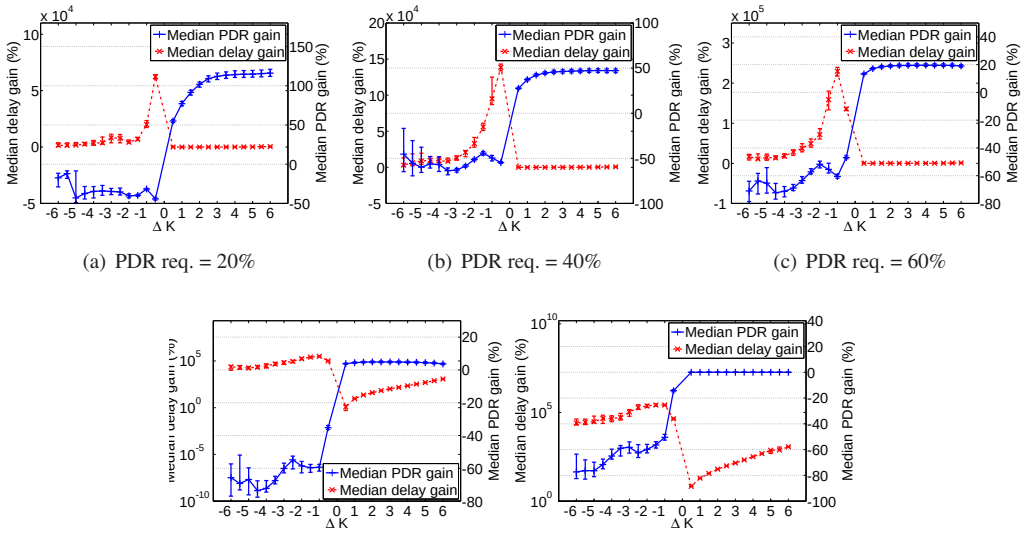

(a) PDR req. = 20%

(b) PDR req. = 40%

(c) PDR req. = 60%

(d) PDR req. = 80%

(e) PDR req. = 99%

Figure 48: Δk vs. performance gain: CSMA, Poisson networks

D. MEASUREMENT-BASED STUDY OF PRK- AND SINR-BASED SCHEDULING WITH THE GREEDYPHYSICAL AND IORDER ALGORITHMS

Besides the LQF-based scheduling algorithm as discussed in Section 6.2, here we compare PRK- and SINR-based scheduling using the GreedyPhysical [Brar et al. 2006; Wang et al. 2006] and the iOrder [Che et al. 2011] scheduling algorithms. The measurement methodology is the same as that in Section 6.1.

GreedyPhysical algorithm. The GreedyPhysical algorithm is similar to the LQF algorithm, but, instead of adding links in a decreasing order of the senders' queue length, GreedyPhysical selects non-interfering links for a slot in a decreasing of their interference numbers. The interference number of a link ℓ is defined as the number of other links that do not share any end-node with ℓ but can be interfered by ℓ alone.

For GreedyPhysical scheduling based on the SINR model, we can use the basic GreedyPhysical algorithm [Brar et al. 2006; Wang et al. 2006] without any modification. For GreedyPhysical scheduling based on the PRK model, we can extend the basic GreedyPhysical algorithm to accommodate the special properties of the PRK model, in the same way as we extend the basic LQF algorithm for the PRK model in Section 6.2.

From the testbed experiments, we observe similar phenomena as those with the LQF algorithm. In MoteLab, for instance, Figure 49 shows the PDR and throughput in PRK- and SINR-based scheduling. It shows similar tradeoff between link reliability and network throughput, and it also shows that PRK-based scheduling achieves a throughput similar to what is feasible in SINR-based scheduling while ensuring the required link reliability.

iOrder algorithm. In addressing the drawback that the existing scheduling algorithms do not explicitly consider/optimize the limiting impact of interference in wireless scheduling, we have recently proposed the iOrder scheduling algorithm [Che et al. 2011]. iOrder considers both interference budget and queue length in scheduling, where, given a set of scheduled transmissions in a time slot, the interference budget characterizes the additional interference power that can be tolerated by all the receivers without violating the application requirement on link reliability. When constructing

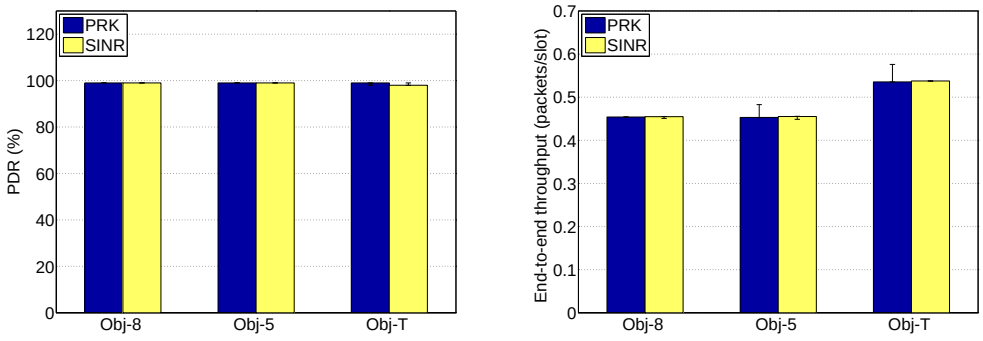

(a) PDR (b) Throughput

Figure 49: PDR and throughput for the GreedyPhysical algorithm in MoteLab

the schedule for a time slot, iOrder first picks a link with the maximum number of queued packets; then iOrder adds links to the slot one at a time in a way that maximizes the interference budget at each step; this process repeats until no additional link can be added to the slot without violating the application requirement on link reliability.

In particular, under the overall framework of ALG_0, iOrder adds links into a slot S_{ℓ_i} using the iOrder-Slot(ℓ_i, E) algorithm [Che et al. 2011], where ℓ_i is the first link added into the slot and E is a set of links such that $\ell_i \notin E$. In iOrder-Slot(ℓ_i, E), a new link ℓ_j that is added into a valid slot-schedule S_{ℓ_i} should satisfy

$$\ell_i = argmax_{l_k \in E_c} I_b(S_{\ell_i} \cup \ell_k),$$

where $I_b(S_{\ell_i})$ is the interference budget of the slot-schedule S_{ℓ_i} and E_c is the set of schedulable links that satisfy the link reliability requirement. It turns out that, given a current valid slot-schedule S_{ℓ_i}, iOrder-Slot(ℓ_i, E) always schedules the link that has the largest s-distance from the links of S_{ℓ_i}, such that the generated schedules in SINR- and PRK-based iOrder algorithms (with the PRK-based scheduling framework as discussed in Section 6.2) are the same. Thus the PDR and throughput in SINR- and PRK-based iOrder algorithms are the same.

REFERENCES

802.15.4A WORKING GROUP, I. IEEE 802.15.4a channel model - final report. Tech. rep.

ARORA, A., RAMNATH, R., ERTIN, E., SINHA, P., BAPAT, S., NAIK, V., KULATHUMANI, V., AND ZHANG ET AL. (30 AUTHORS), H. 2005. Exscal: Elements of an extrem scale wireless sensor network. In *IEEE RTCSA*.

BACCELLI, F. AND BLASZCZYSZYN, B. 2010. Stochastic geometry and wireless networks (volume 2): Applications. *Foundations and Trends in Networking 4,* 1-2, 1–312.

BLOUGH, D. M., DAS, S., RESTA, G., AND SANTI, P. 2008. A framework for joint scheduling and diversity exploitation under physical interference in wireless mesh networks. In *IEEE MASS*.

BRAR, G., BLOUGH, D. M., AND SANTI, P. 2006. Computationally efficient scheduling with the physical interference model for throughput improvement in wireless mesh networks. In *ACM MobiCom*.

BRAR, G., BLOUGH, D. M., AND SANTI, P. 2008. The SCREAM approach for efficient distributed scheduling with physical interference in wireless mesh networks. In *ICDCS*.

CHAFEKAR, D., KUMAR, V. A., MARATHE, M. V., PARTHASARATHY, S., AND SRINIVASAN, A. 2008. Approximation algorithms for computing capacity of wireless networks with sinr constraints. In *IEEE INFOCOM*.

CHE, X., JU, X., AND ZHANG, H. 2011. The case for addressing the limiting impact of interference on wireless scheduling. In *IEEE ICNP*.

CHEN, D., NIXON, M., AND MOK, A. 2010. *Wireless*HART*: Real-Time Mesh Network for Industrial Automation*. Springer.

CHINTALAPUDI, K. AND VENKATRAMAN, L. 2008. On the design of mac protocols for low-latency hard real time latency applications over 802.15.4 hardware. In *ACM/IEEE IPSN*.

CHOI, J. I., JAIN, M., KAZANDJIEVA, M. A., AND LEVIS, P. 2010. Granting silence to avoid wireless collisions. In *IEEE ICNP*.

GOLLAKOTA, S. AND KATABI, D. 2008. ZigZag decoding: Combating hidden terminals in wireless networks. In *ACM SIGCOMM*.

GUPTA, P. AND KUMAR, P. R. 2000. The capacity of wireless networks. *IEEE Transactions on Information Theory 46,* 2.

HALPERIN, D., ANDERSON, T., AND WETHERALL, D. 2008. Taking the sting out of carrier sense: Interference cancellation for wireless LANs. In *ACM MobiCom*.

HELLERSTEIN, J., DIAO, Y., PAREKH, S., AND TILBURY, D. M. 2004. *Feedback Control of Computing Systems*. Wiley-IEEE Press.

JOO, C., LIN, X., AND SHROFF, N. B. 2008. Understanding the capacity region of the greedy maximal scheduling algorithm in multi-hop wireless networks. In *IEEE INFOCOM*.

JU, X., ZHANG, H., AND SAKAMURI, D. 2012. NetEye: A user-centered wireless sensor network testbed for high-fidelity, robust experimentation. *International Journal of Communication Systems (Wiley) 25,* 9, 1213–1229.

KATZ, B., VOLKER, M., AND WAGNER, D. 2008. Link scheduling in local interference models. In *AlgoSensors*.

LE, L. B., MODIANO, E., JOO, C., AND SHROFF, N. B. 2010. Longest-queue-first scheduling under SINR interference model. In *ACM MobiHoc*.

LI, L. E., ALIMI, R., SHEN, D., VISWANATHAN, H., AND YANG, Y. R. 2010. A general algorithm for interference alignment and cancellation in wireless networks. In *IEEE INFOCOM*.

MA, H., ALAZEMI, H. M., AND ROY, S. 2005. A stochastic model for optimizing physical carrier sensing and spatial reuse in wireless ad hoc networks. In *IEEE MASS*.

MAHESHWARI, R., CAO, J., AND DAS, S. 2009. Physical interference modeling for transmission scheduling on commodity wifi hardware. In *IEEE INFOCOM miniconference*.

MAHESHWARI, R., JAIN, S., AND DAS, S. 2008. A measurement study of interference modeling and scheduling in low-power wireless networks. In *ACM SenSys*.

MENON, R., BUEHRER, R. M., AND REED, J. H. 2006. Impact of exclusion region and spreading in spectrum-sharing ad hoc networks. In *ACM Workshop on Technology and Policy for Accessing Spectrum*.

MOSCIBRODA, T., WATTENHOFER, R., AND WEBER, Y. 2006. Protocol design beyond graph based models. In *ACM HotNets*.

NIU, W., LI, J., AND TALTY, T. 2008. Intra-vehicle UWB channel measurements and statistical analysis. In *IEEE GlobeCom*.

RAPPAPORT, T. 2002. *Wireless Communications*. Prentice-Hall, Upper Saddle River, NJ.

RHEE, I., WARRIER, A., MIN, J., AND XU, L. 2006. DRAND: Distributed randomized TDMA scheduling for wireless ad hoc networks. In *ACM MobiHoc*.

SHA, M., XING, G., ZHOU, G., LIU, S., AND WANG, X. 2009. C-MAC: Model-driven concurrent medium access control for wireless sensor networks. In *IEEE INFOCOM*.

SHARMA, G., MAZUMDAR, R. R., AND SHROFF, N. B. 2006. On the complexity of scheduling in wireless networks. In *ACM MobiCom*.

SHARMA, G., SHROFF, N., AND MAZUMDAR, R. 2006. Maximum weighted matching with interference constraints. In *IEEE PERCOMW*.

SHI, Y., HOU, Y. T., LIU, J., AND KOMPELLA, S. 2009. How to correctly use the protocol interference model for multi-hop wireless networks. In *ACM MobiHoc*.

SOHRABI, K., MANRIQUEZ, B., AND POTTIE, G. J. 1999. Near ground wideband channel measurement. In *IEEE VTC*.

STOYAN, D., KENDALL, W. S., AND MECKE, J. 1995. *Stochastic Geometry and its applications*. Wiley.

TABET, T. AND KNOPP, R. 2004. Spatial throughput of multi-hop wireless networks under different retransmission protocols. In *Allerton*.

IEEE 802.15.4. 2006. Wireless medium access control (MAC) and physical layer (PHY) specifications for low-rate wireless personal area networks (WPANs). IEEE Std 802.15.4-2006.

ISA SP100.11A. `http://www.isa.org//MSTemplate.cfm?MicrositeID=1134\&CommitteeID=6891`.

TOBAGI, F. AND KLEINROCK, L. 1975. Packet switching in radio channels: Part II–the hidden terminal problem in carrier sense multiple-access and the busy-tone solution. *IEEE Transactions on Communications COM-23,* 12, 1417–1433.

WANG, W., WANG, Y., LI, X.-Y., SONG, W.-Z., AND FRIEDER, O. 2006. Efficient interference-aware TDMA link scheduling for static wireless networks. In *AMC MobiCom*.

WEBER, S., YANG, X., ANDREWS, J. G., AND DE VECIANA, G. December 2005. Transmission capacity of wireless ad hoc networks with outage constraints. *IEEE Transactions on Information Theory 51,* 12.

WERNER-ALLEN, G., SWIESKOWSKI, P., AND WELSH, M. 2005. Motelab: A wireless sensor network testbed. In *IEEE/ACM IPSN/SPOTS*.

YEDAVALLI, K. AND KRISHNAMACHAR, B. 2008. 'enhancement of the IEEE 802.15.4 MAC protocol for scalable data collection in dense sensor networks. In *International Symposium on Modeling and Optimizationin Mobile, Ad Hoc, and Wireless Networks*.

YI, Y., VECIANA, G. D., AND SHAKKOTTAI, S. 2007. On optimal MAC scheduling with physical interference model. In *IEEE INFOCOM*.

YING, L. AND SHAKKOTTAI, S. 2009. Scheduling in mobile ad hoc networks with topology and channel-state uncertainty. In *IEEE INFOCOM*.

ZHANG, H., ARORA, A., RI CHOI, Y., AND GOUDA, M. 2007. Reliable bursty convergecast in wireless sensor networks. *Computer Communications (Elsevier), Special Issue on Sensor-Actuator Networks 30,* 13.

ZHANG, H., ARORA, A., AND SINHA, P. May 2009. Link estimation and routing in sensor network backbones: Beacon-based or data-driven? *IEEE Transactions on Mobile Computing 8,* 5, 653 – 667.

ZHANG, H., CHE, X., LIU, X., AND JU, X. August 2012. Adaptive instantiation of the protocol interference model in wireless networked sensing and control. Tech. Rep. WSU-CS-DNC-TR-12-01, Wayne State University (`https://sites.google.com/site/dnctrs/DNC-TR-12-01.pdf`).

ZHANG, H., LI, C., LIU, X., CHEN, Y., CHE, X., LIN, F., WANG, L. Y., AND YIN, G. 2012. PRK-based scheduling for predictable link reliability in wireless networked sensing and control. Tech. Rep. DNC-TR-12-02 (`https://sites.google.com/site/dnctrs/DNC-TR-12-02.pdf`), Wayne State University.

ZHANG, Y. AND BROWN, A. K. 2008. Data rate for ds-uwb communication systems in wireless personal area networks. In *ICUWB*.

ZHOU, G., HE, T., KRISHNAMURTHY, S., AND STANKOVIC, J. 2006. Models and solutions for radio irregularity in wireless sensor networks. *ACM Transactions on Sensor Networks 2,* 2.

ZHOU, G., HE, T., STANKOVIC, J. A., AND ABDELZAHER, T. 2005. RID: Radio interference detection in wireless sensor networks. In *IEEE INFOCOM*.

ZUNIGA, M. AND KRISHNAMACHARI, B. 2007. An analysis of unreliability and asymmetry in low-power wireless links. *ACM Transactions on Sensor Networks 3,* 2.